

Skin-Friction and Forced Convection from Rough and Smooth Plates

Aubrey G. Jaffer
e-mail: agj@alum.mit.edu

Abstract

Since the 1930s, models for skin-friction drag from plates with rough surfaces have been based on analogy to flow within pipes having rough interiors. However, this analogy fails at small Reynolds number (Re) flow rates. Significant discrepancies from the pipe analogy at small Re were found by the rough plate experiments of Hama (1954) and Pimenta, Moffat, and Kays (1975).

The present work derives exact formulas for a plate's skin-friction drag coefficient and turbulent forced convection given its root-mean-squared height-of-roughness, and Re bounds from the spatial frequency spectrum of its roughness. These formulas are in close agreement with the Mills-Hang (1983) formula, the Pimenta et al measurements, and experiments conducted by the present author.

The present work also derives an exact formula for skin-friction coefficient of a smooth plate; this formula is in very close agreement with measurements from Smith and Walker (1959) and Spalding and Chi (1964) spanning 4 decades of Re. Its new formula for turbulent forced convection is in agreement with Lienhard (2020), while expanding the range to all fluid Prandtl numbers.

This research did not receive any specific grant from funding agencies in the public, commercial, or not-for-profit sectors.

Table of contents

1. <i>Introduction</i>	2
2. <i>Prior work</i>	3
3. <i>Rough turbulence</i>	4
4. <i>Profile roughness</i>	4
5. <i>Self-similar ramp permutations</i>	5
6. <i>Roughness travel</i>	6
7. <i>Skin-friction</i>	7
8. <i>Spectral roughness</i>	9
9. <i>Periodic roughness</i>	10
10. <i>Periodic smoothness</i>	12
11. <i>Local skin-friction</i>	13
12. <i>Forced convection</i>	14
13. <i>Periodic versus self-similar roughness</i>	18
14. <i>Fully rough regime</i>	18
15. <i>Transitional rough regime</i>	19
16. <i>Convection measurements</i>	20
17. <i>Discussion</i>	22
18. <i>Conclusions</i>	23
19. <i>Nomenclature</i>	24
20. <i>References</i>	25

arXiv:1810.05743v12 [physics.flu-dyn] 31 Jan 2021

1. Introduction

Skin-friction drag is the pressure opposing flow due to viscous dissipation of turbulence generated by that flow along a surface. Skin-friction is important to the fluid dynamics of vehicles and turbines. The related phenomenon of forced convection has application to modeling weather and the thermal behavior of buildings.

The present work uses the terms “skin-friction” and “skin-friction drag” interchangeably; also “rough” and “fully rough”; also “smooth” and “hydraulically smooth”; also “turbulence” and “turbulent flow”.

In 1934 Prandtl and Schlichting published *Das Widerstandsgesetz rauher Platten* (*The Resistance Law for Rough Plates* [1]); it brilliantly infers a relation for skin-friction resistance for rough plates from their analysis of Nikuradse’s [2] measurements of sand glued inside pipes (“sand-roughness”). At the conclusion of the paper they write:

“The resistance law just derived for rough plates has chiefly validity for a very specific type of roughness, namely a smooth surface to which sand grains have been densely attached and where the Nikuradse pipe results have been taken as the basis. . .

A single roughness parameter (the relative roughness) will in all likelihood no longer answer the purpose in continued investigations of the roughness problem.”

Hama [3] describes three challenges to the pipe-plate analogy:

“Now there is no obvious reason why pipe flow and boundary-layer flow should be identical or even similar. First, a pressure gradient is essential for flow through a pipe but not along a plate. Second, pipe flow is confined and perforce uniform, while flow along a plate develops semi-freely and bears no such a priori guarantee of displaying similar velocity profiles at successive sections. Finally, the diameter and roughness size are the only geometrical dimensions of established flow in pipes, whereas at least three linear quantities are necessary to characterize the boundary layer.”

Hama attempts to confirm the pipe-plate analogy with measurements of wire screens affixed to smooth plates, but concludes that it is confirmed only for large Reynolds number (Re) flow rates.

Flow at the plate surface has zero velocity. The “boundary layer” is flow near the surface which has velocity different from the bulk flow velocity v .

Roughness in prior works [1, 2, 3, 4, 5, 6, 7, 8] is reported in sand-roughness k_S , the height of “coarse and tightly placed roughness elements such as for example coarse sand grains glued on the surface” [6].

A machined analogue to sand-roughness, the plate tested by Pimenta, Moffat, and Kays [4] was composed of 11 layers of densely packed metal balls 1.27 mm in diameter “arranged such that the surface has a regular array of hemispherical roughness elements.” The reported sand-roughness of the plate was $k_S = 0.79$ mm. Pimenta et al write that, while the agreement of their data with the Prandtl-Schlichting plate model is “rather good” in the fully rough regime, their apparatus doesn’t have the same behavior as “Nikuradse’s sand-grain pipe flows in the transition region”.

The “fully rough regime” denotes a mode of (large Re) flow in pipes having rough interiors which has larger skin-friction coefficients than the same flow inside smooth pipes. For sand-roughness, the fully rough regime has a constant skin-friction coefficient versus flow rate Re.

Taking the wake component of the velocity profile into account, Mills and Hang [5] created a model improving the match to Pimenta et al data at large Re, but didn’t address the discrepancies at small Re.

The discrepancies at small Re, the search for an additional roughness parameter, and the reliance on sand-roughness motivate a new theoretical analysis of flow along plate roughness in terms of a traceable roughness metric. Two widely used traceable roughness metrics are root-mean-squared (RMS) and arithmetic-mean height-of-roughness. For an elevation function $z(x, y)$ defined on area A with a convex perimeter, its mean elevation \bar{z} and RMS height-of-roughness ε are:

$$\bar{z} = \int_A z dA / \int_A dA \quad \varepsilon = \sqrt{\int_A |z - \bar{z}|^2 dA / \int_A dA} \quad (1)$$

Arithmetic-mean height-of-roughness is also defined using mean elevation \bar{z} :

$$\int_A |z - \bar{z}| dA / \int_A dA \quad (2)$$

2. Prior work

There are several formulas for skin-friction coefficient in the fully rough regime (large Re).

In *Boundary-layer theory* [6] Prandtl and Schlichting give formulas for fully rough local (c'_f) and plate average (c_f) skin-friction coefficient for a rough flat plate in terms of its sand-roughness k_S and the distance x along the plate in the direction of flow up to the characteristic-length L (plate length in the flow direction):

$$c'_f = \left(2.87 + 1.58 \log_{10} \frac{x}{k_S} \right)^{-2.5} \quad x \leq L \quad (3)$$

$$c_f = \left(1.89 + 1.62 \log_{10} \frac{L}{k_S} \right)^{-2.5} \quad 10^2 < \frac{L}{k_S} < 10^6 \quad (4)$$

Mills and Hang [5] give a formula (5) which is more accurate than formula (3) on the local skin-friction measurements from Pimenta et al [4]. Their local (C_f) and average (C_D) coefficient formulas are:

$$C_f = \left(3.476 + 0.707 \ln \frac{x}{k_S} \right)^{-2.46} \quad x \leq L \quad (5)$$

$$C_D = \left(2.635 + 0.618 \ln \frac{L}{k_S} \right)^{-2.57} \quad 750 < \frac{L}{k_S} < 2750 \quad (6)$$

White [7] gives a formula for fully rough local skin-friction coefficient. $\text{Re}_x = \text{Re} x/L$ is the local Reynolds number.

$$C_f = \left(1.4 + 3.7 \log_{10} \frac{x}{k_S} \right)^{-2} \quad \frac{x}{k_S} > \frac{\text{Re}_x}{1000} \quad (7)$$

White is also the source of a widely used formula for turbulent skin-friction coefficient for smooth plates:

$$C_f(\text{Re}_x) = \frac{0.455}{\ln^2(0.06 \text{Re}_x)} \quad (8)$$

Mills and Hang [5] derived the average formula (6) from the local formula (5) by fitting a curve to the result of the numerical integration in formula (9):

$$C_D \left(\frac{L}{k_S} \right) = \frac{k_S}{L - L_0} \int_{L_0/k_S}^{L/k_S} C_f(x) dx \quad (9)$$

The local formulas (3), (5), and (7) each have a singularity when the expression containing the logarithm is zero. The lower limit of integration (L_0/k_S) must be large enough to avoid this, but the lower limit isn't revealed in the prior work. The averaging formula (9) is quite sensitive to the lower limit because the largest value of the local formula occurs there.

For the Mills-Hang formula (5), with a lower bound of 1.6 and initial $dx/k_S = 0.01$, integration of the local C_f is within $\pm 0.5\%$ of the average C_D in formula (6) over the range $200 < x/k_S < 200 \times 10^3$.

For the Prandtl-Schlichting formula (3), with a lower bound of 0.5 and initial $dx/k_S = 0.5$, integration of the local c'_f is within $\pm 0.5\%$ of the average c_f in formula (4) over the range $200 < x/k_S < 200 \times 10^3$.

Churchill [8] compares 8 formulas from various sources with the data from Pimenta et al [4]; it doesn't find any to be significantly superior to the Mills-Hang local formula (5). Churchill has different methods for computing the average (mean) skin-friction C_m from local C_f for smooth and rough surfaces, respectively:

$$C_m = C_f \frac{1 - 4.516\sqrt{C_f}}{1 - 7.965\sqrt{C_f} + 21.52 C_f} \quad C_m = C_f \frac{1 - 4.516\sqrt{C_f}}{1 - 7.965\sqrt{C_f}} \quad (10)$$

The utility of the formulas (3, 4, 5, 6, 7) would be greater if they were defined in terms of a roughness metric applicable to any surface, such as root-mean-squared (RMS) or arithmetic-mean height-of-roughness.

Afzal, Seena, and Bushra [9] fit 5.333 for the RMS to sand-roughness conversion factor and 6.45 for arithmetic-mean to sand-roughness in pipes.

Flack, Schultz, Barros, and Kim [10] measured skin-friction from grit-blasted surfaces in a duct. They write "The root-mean-square roughness height is shown to be most strongly correlated with the equivalent sand-roughness height (k_S) for the grit-blasted surfaces."

3. Rough turbulence

Forced flow along a plate with a rough surface is different in character from forced flow along a smooth surface because roughness disrupts what would otherwise be a viscous sub-layer adjacent to the plate. Lienhard and Lienhard [11] teach: “Even a small wall roughness can disrupt this thin sublayer, causing a large decrease in the thermal resistance (but also a large increase in the wall shear stress).”

Because boundary layers are disrupted by roughness, the present work models the effect of roughness on flow as a series of disruptions instead of a continuous boundary layer.

To guarantee that the turbulence generated by flow along a rough surface is rough turbulent, there should be disruptive roughness along the full length of the plate. The turbulent boundary-layer depth along a smooth plate increases as $x^{4/5}$, where x is the distance from its leading edge. Roughness whose envelope height increases linearly with x can disrupt nascent boundary layers repeatedly along the entire plate.

Although vortexes can arise in two-dimensional systems, turbulence is a three-dimensional phenomenon. Its random velocity fluctuations must be isotropic at all except the coarsest length scales. To guarantee this, the roughness should be at least “weakly isotropic”; rotating the plate within its plane shouldn’t substantially affect the behavior of the system. A plate surface composed of parallel edge-to-edge ridges and valleys wouldn’t satisfy this criterion.

4. Profile roughness

Simpler than surface roughness, much can be learned from planar roughness profiles.

Let “profile roughness” be a function $z(x)$ where $0 \leq x \leq L$ is distance from the leading edge in the direction of flow up to plate length L . Given a roughness profile $z(x)$, its mean elevation \bar{z} and RMS height-of-roughness ϵ are:

$$\bar{z} = \frac{1}{L} \int_0^L z(x) dx \quad \epsilon = \sqrt{\frac{1}{L} \int_0^L |z(x) - \bar{z}|^2 dx} \quad (11)$$

Let “self-similar profile roughness” be a profile roughness function $z(x)$ with (integer) branching factor $n \geq 2$ such that the RMS height-of-roughness of $z(x)$ over an interval $x_0 < x < x_n$ is n times the RMS height-of-roughness of $z(x)$ over each equally divided sub-interval $x_t < x < x_{t+1}$ for $0 \leq t < n$ at a succession of scales converging to zero. Note that each $z(x_t)$ value contributes to its parent interval height-of-roughness, but not to any sub-interval.

A consequence of this definition is that the ratio of the length of an interval to the RMS height-of-roughness of z over that interval will be invariant over its succession of scales.

Of particular interest are self-similar roughness profiles which are permutations of the linear ramp $z(x) = \varsigma x/L$ from $x = 0$ to $x = L$, where ς is the elevation of the highest peak. Every elevation from 0 to ς occurs exactly once in a ramp-permutation. The RMS height-of-roughness calculation (11) depends only on the z values, not their relation to x . Hence, for all ramp-permutations:

$$\epsilon = \sqrt{\frac{1}{L} \int_0^L \left[\frac{\varsigma x}{L} - \frac{\varsigma}{2} \right]^2 dx} = \frac{\varsigma}{\sqrt{12}} \quad (12)$$

All ramp-permutations have arithmetic-mean height-of-roughness $\varsigma/4$:

$$\frac{1}{L} \int_0^L \left| \frac{\varsigma x}{L} - \frac{\varsigma}{2} \right| dx = \frac{\varsigma}{4} \quad (13)$$

5. Self-similar ramp permutations

A self-similar integer sequence $Y(t, w)$ of integers $0 \leq t < w = n^q$ allows self-similar behavior to be explored with a finite approximation. A roughness profile can be constructed from a sequence by $z(x) = (\varsigma/w) Y(\lfloor wx/L \rfloor, w)$. The following three examples are bisected ($n = 2$) ramp-permutation sequences.

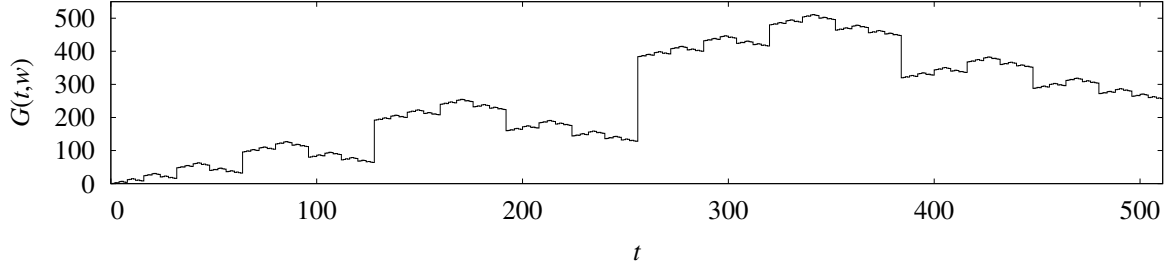


Figure 1 Gray-code profile roughness

The integer Gray-code sequence $G(t, w)$ shown in Figure 1 is a self-similar sequence defined by recurrence:

$$G(t, w) = \begin{cases} t, & \text{if } w = 1; \\ w + G(w - 1 - (t \bmod w), w/2), & \text{if } \lfloor t/w \rfloor = 1; \\ G(t \bmod w, w/2), & \text{otherwise.} \end{cases} \quad (14)$$

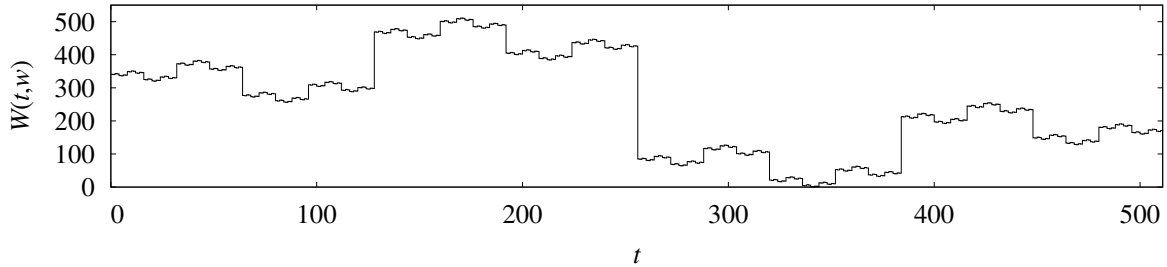


Figure 2 wiggliest self-similar profile roughness

The integer sequence $W(t, w)$ defined by recurrence (15) is shown in Figure 2; it reverses direction at each bifurcation, yielding a wiggliest possible self-similar ramp-permutation sequence.

$$W(t, w) = \begin{cases} t, & \text{if } w = 1; \\ \lfloor t/w \rfloor w + W(w - 1 - (t \bmod w), w/2), & \text{otherwise.} \end{cases} \quad (15)$$

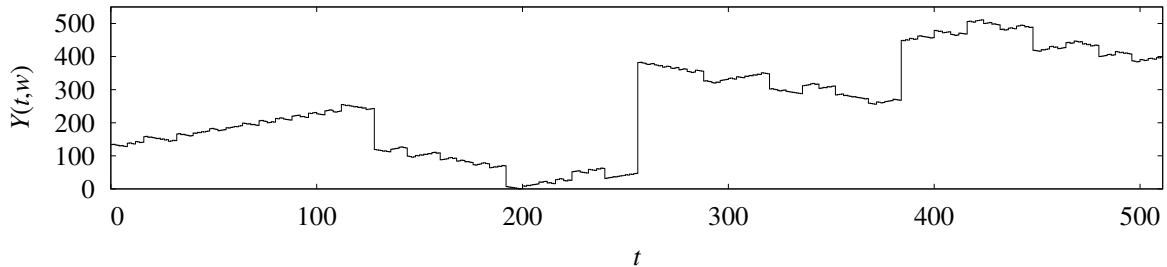


Figure 3 random reversal bifurcation profile roughness

Figure 3 shows an integer sequence generated by recursive-descent, randomly reversing or not at each bifurcation (16); its roughness is self-similar by the definition of self-similar profile roughness in Section 4.

$$Y(t, w) = \begin{cases} t, & \text{if } w = 1; \\ w + Y(w - 1 - (t \bmod w), w/2), & \text{with probability 0.5;} \\ Y(t \bmod w, w/2), & \text{otherwise.} \end{cases} \quad (16)$$

For a given $w = 2^q \geq 4$, there are $2^w = 2^{(2^q)}$ distinct self-similar ramp-permutation sequences, but only 2 distinct ramp and 2 distinct wiggliest sequences.

6. Roughness travel

In the conversion of flow to rough turbulence, particles of fluid must move in directions not parallel to the bulk flow. Such movement will result from deflection of flow by roughness peaks, ridges, and valleys; the amount of turbulence induced grows with the height-of-roughness.

let “run” be the t -axis and “friction” be the Y -axis.

For an integer ramp-permutation sequence $Y(t, w)$, the sum of the (dimensionless) lengths of all run segments is $w - 1 = 2^q - 1$. The sum of the absolute value of each friction segment length is:

$$\sum_{t=0}^{2^q-2} |Y(t, 2^q) - Y(t+1, 2^q)| \quad (17)$$

If a particle of fluid were to trace the ramp-permutation sequence $Y(t, w)$ from $t = 0$ to $t = w - 1$, then $w - 1$ is the run distance it would travel, while formula (17) is the friction distance.

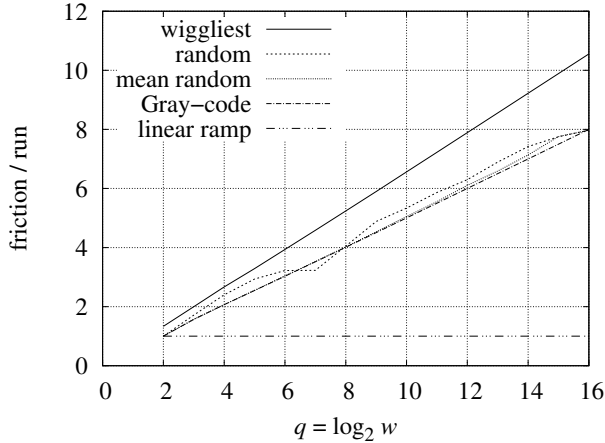


Figure 4 travel along profile roughness

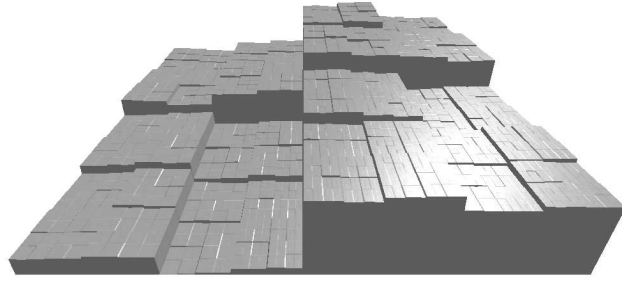


Figure 5 random reversal ramp surface

Figure 4 shows the friction travel to run travel ratio versus q , the base-2 logarithm of w . The slope is 0 for the linear ramp, $1/2$ for the Gray-code, approximately $1/2$ for the random reversal cases, and $2/3$ for the wiggliest roughness W . The friction segments in the wiggliest sequence in Figure 2 are indeed longer than those in Figures 1 and 3.

A wiggliest roughness sequence $W(t, w)$ is an extreme case; it reverses friction direction at each increment of run (t). For each wiggliest roughness sequence with $w \geq 4$ there are $2^{w-1} - 2$ other random reversal roughness sequences. The linear ramp is the opposite extreme. For each linear ramp sequence there are $2^{w-1} - 2$ other random reversal sequences. Going forward, $W(t, w)$ and linear ramps are excluded as outliers.

In Figure 4, the friction to run ratios for Gray-code and random reversal sequences are close to:

$$\frac{q}{2} \equiv \frac{\log_2 w}{2} \quad (18)$$

$Y(t, w)$, t , and w are dimensionless. The friction to run ratio (18) needs to be reformulated in terms of the height-of-roughness. Turning to dimensional analysis, the argument to \log_2 must be dimensionless, involve ϵ , and be greater than 1, so that the logarithm will be positive. This ratio must increase with increasing ϵ ; thus, ϵ and the logarithm will be in denominators, yielding a friction travel to run travel ratio:

$$\frac{2}{\log_2(L/\epsilon)} \quad (19)$$

Scaling formula (19) by $1/\sqrt{12}$ (from formula (12)) converts formula (19) into the ratio of RMS friction travel to run travel:

$$\frac{1}{\sqrt{12}} \frac{2}{\log_2(L/\epsilon)} = \frac{1}{\sqrt{3} \log_2(L/\epsilon)} \quad (20)$$

Newberry and Savage [12] demonstrate that some self-similar systems which are modeled using continuous power-law probability distributions can be modeled using discrete power-law distributions.

The present work uses their idea in reverse. The conversion of flow into turbulence by contact with discrete self-similar $n = 2$ roughness was modeled by formula (20); the skin-friction drag of turbulence generation by a random self-similar roughness will be inferred using a random variable.

Instead of summing $|Y(t, 2^q) - Y(t + 1, 2^q)|$ as in formula (17), the analogous mean field theory is to integrate $Z > 0$, a continuous random variable having a Pareto distribution where the frequency of Z is inversely proportional to Z^2 :

$$1 / \left[\sqrt{3} \int_{\epsilon}^L \frac{Z}{Z^2} dZ \right] = \frac{1}{\sqrt{3} \ln(L/\epsilon)} \quad (21)$$

Travel along profile roughness is a planar path. Along self-similar surface roughness, an example of which is shown in Figure 5, the path of a particle can be 3-dimensional. In the generalization of formula (20) to random self-similar roughness in formula (21), the profile height-of-roughness ϵ is replaced with the surface height-of-roughness ϵ defined in formula (1). As with profile RMS height-of-roughness, the surface RMS height-of-roughness of any permutation of the linear ramp from 0 to ς is $\varsigma/\sqrt{12}$. Therefore, the $1/\sqrt{3}$ coefficient doesn't change with the substitution of ϵ for ϵ in formula (21).

7. Skin-friction

The skin-friction coefficient f_C is the ratio of the shear stress τ , which is primarily skin-friction drag when $L/\epsilon \gg 1$, to the flow's kinetic energy density $\rho v^2/2$, where v is bulk flow velocity and ρ is fluid density:

$$f_C = \frac{\tau}{\rho v^2/2} \quad (22)$$

f_C is dimensionless; both τ and $\rho v^2/2$ have units of pressure, $\text{kg}/(\text{m} \cdot \text{s}^2)$.

Considering the run travel and friction travel with respect to time lets formula (21) serve as the ratio of friction velocity v^* to bulk flow velocity v . Hence, multiplication by formula (21) converts bulk flow velocity v to friction velocity v^* , from which τ is derived:

$$v^* = \frac{v}{\sqrt{3} \ln(L/\epsilon)} \quad \tau = \frac{\rho v^{*2}}{2} = \frac{\rho v^2}{6 \ln^2(L/\epsilon)} \quad \frac{L}{\epsilon} \gg 1 \quad (23)$$

Combining equations (22) and (23) yields the formula for the average skin-friction coefficient f_C of a weakly isotropic self-similar rough surface:

$$f_C = \frac{1}{3 \ln^2(L/\epsilon)} \quad \frac{L}{\epsilon} \gg 1 \quad (24)$$

Prandtl and Schlichting [1] calculate $\tau = \rho v^{*2}$, not $\tau = \rho v^{*2}/2$. As a result, Prandtl-Schlichting c_f is about twice f_C of formula (24). Pimenta et al [4] and Mills and Hang [5] use $c_f/2$ as skin-friction coefficient.

This derivation can be extended to smooth plates.

For a given Re there must be a ratio L/ϵ so large that a length L plate with roughness ϵ behaves as a smooth surface. The roughness Reynolds number Re_ϵ is the dimensionless friction velocity:

$$\text{Re}_\epsilon = \frac{v^* \epsilon}{\nu} = \frac{v}{\sqrt{3} \ln(L/\epsilon)} \frac{\epsilon}{\nu} = \frac{\text{Re}}{\sqrt{3} [L/\epsilon] \ln(L/\epsilon)} \quad (25)$$

where ν is the fluid kinematic viscosity and $\text{Re} = Lv/\nu$.

The Re at which rough plate skin-friction transitions to smooth plate skin-friction will have the same Re_ϵ value at all $L/\epsilon \gg 1$. Combining $\text{Re}_\epsilon = 1$ with formula (25) relates Re to L/ϵ at transition:

$$\text{Re} = \sqrt{3} \frac{L}{\epsilon} \ln \frac{L}{\epsilon} \quad (26)$$

Relation (26) between Re and L/ε suggests that the smooth turbulent skin-friction coefficient can be inferred from formulas (24) and (26). However, there being no actual surface roughness, f_C formula (24) must be adapted for this use; the L/ε argument to f_C is scaled by $1/e$; the value of f_C is scaled by $\sqrt[3]{2}$:

$$f_{C\sigma} = \sqrt[3]{2} f_C \left(\frac{L}{e\varepsilon} \right) = \sqrt[3]{2} \left[\frac{1}{3} \ln^{-2} \frac{L}{e\varepsilon} \right] \quad Re = \sqrt{3} \frac{L}{\varepsilon} \ln \frac{L}{\varepsilon} \quad (27)$$

L/ε can be eliminated from formulas (27) using the Lambert W function. The inverse of $\vartheta = \varphi \ln(\varphi)$ is $\varphi = \exp(W_0(\vartheta))$, where W_0 is the smallest positive branch of the Lambert W function.

$$f_{C\sigma}(Re) = \frac{\sqrt[3]{2}}{3} \ln^{-2} \left(\frac{\exp(W_0(Re/\sqrt{3}))}{e} \right) = \frac{\sqrt[3]{2}/3}{[W_0(Re/\sqrt{3}) - 1]^2} \quad Re \gg \sqrt{3}e \quad (28)$$

Euler's number $e = \exp(1)$ is a fixed point of $\varphi \ln(\varphi)$ and its inverse, $\exp(W_0(\vartheta))$. Dividing L/ε by e moves the Re lower bound from 0 to $\sqrt{3}e \approx 4.71$. The coefficient $\sqrt[3]{2}/3 \approx 0.4200$; $\sqrt[3]{2}$ is related to $\sqrt[2]{3}$.

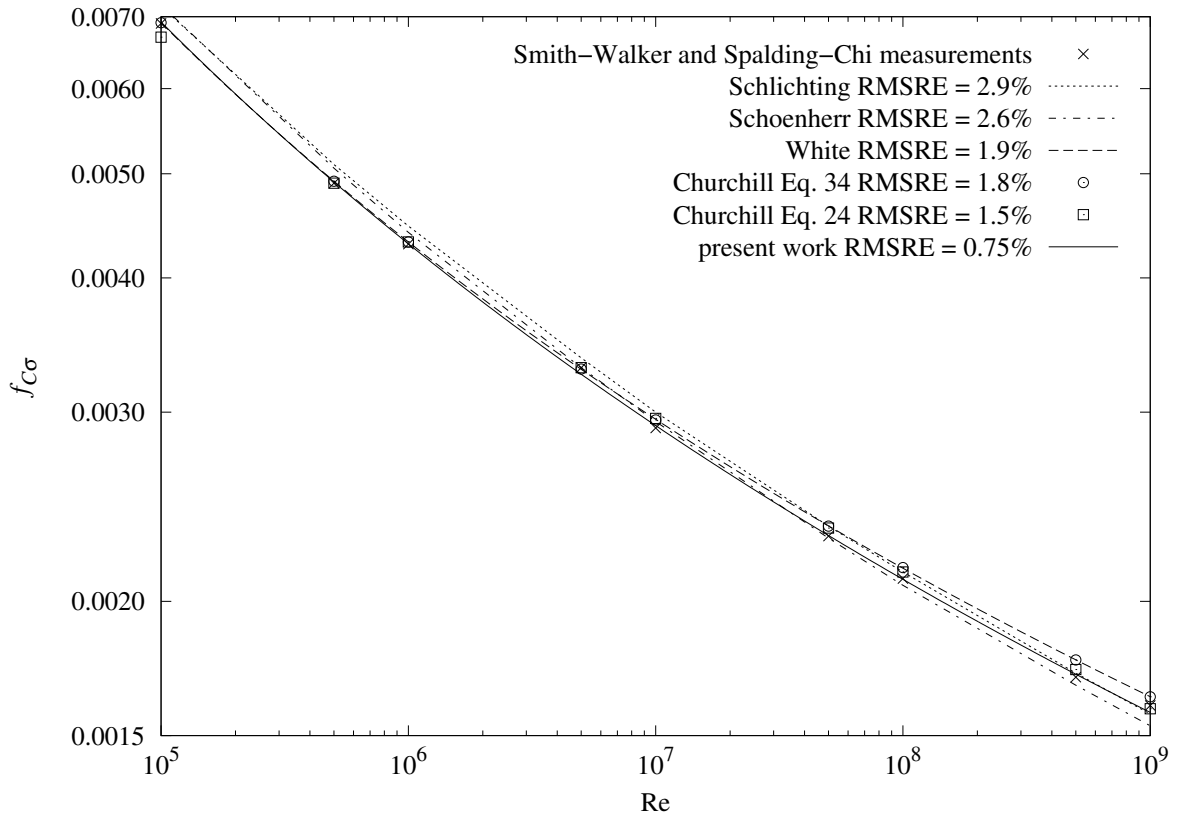


Figure 6 average $f_{C\sigma}$ versus Re of smooth plate

Churchill [8] compares smooth turbulent skin-friction coefficient formulas from various sources with measured data from Smith and Walker [13], and Spalding and Chi [14]. Average formula and data values provided by Churchill are shown in Figure 6. The “present work” formula (28) has 0.75% RMS relative error (RMSRE) from the “Smith-Walker and Spalding-Chi measurements”.

RMSRE gauges the fit of a formula to data having a wide dynamic range, giving each measurement equal weight. The RMS error of $f(x)$ relative to $g(x)$ is:

$$\sqrt{\frac{1}{n} \sum_{j=1}^n \left| 1 - \frac{f(x_j)}{g(x_j)} \right|^2} \quad (29)$$

8. Spectral roughness

There is a profound connection between the discrete Fourier transform X_j of a roughness sequence $Y(t, w)$ and its RMS height-of-roughness ϵ :

$$X_j = \sum_{t=0}^{w-1} Y(t, w) \exp\left(\frac{-2\pi i j t}{w}\right) \quad \epsilon = \sqrt{\frac{1}{w} \sum_{j=1}^{w-1} |X_j|^2} \quad (30)$$

Note that the constant term, X_0 , which is the mean value of Y , isn't included in the sum for ϵ .

When X_j is computed as the Riemann sum (30) over rectangles sampled only at their left edges, it underestimates the magnitude of the sum and introduces a phase shift. S_j in formula (31) is the compensated spectrum; $|S_j/X_j|$ decreases from $\pi/2 \approx 1.57$ at $j = 0$ to 1 at the Nyquist frequency $j = w/2$.

$$S_j = X_j \frac{w}{2j} \sin \frac{\pi j}{w} \exp \frac{\pi i j}{w} \quad 0 < j \leq \frac{w}{2} \quad (31)$$

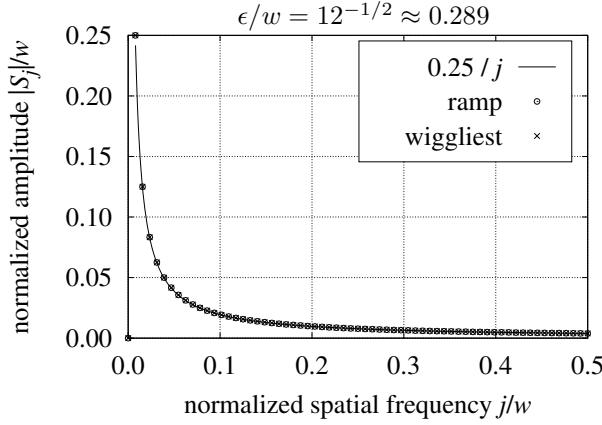


Figure 7 wiggliest and ramp spectra

Figure 7 shows the $|S_j|/w$ spectra of the wiggliest (Figure 2) and ramp profiles. The amplitudes of the wiggliest and ramp spectra are identical; the difference in their spectra is the phase of the complex-valued S_j ; the ramp phases are all $+90^\circ$ or all -90° ; the wiggliest phases are an unequal mixture of $+90^\circ$ and -90° .

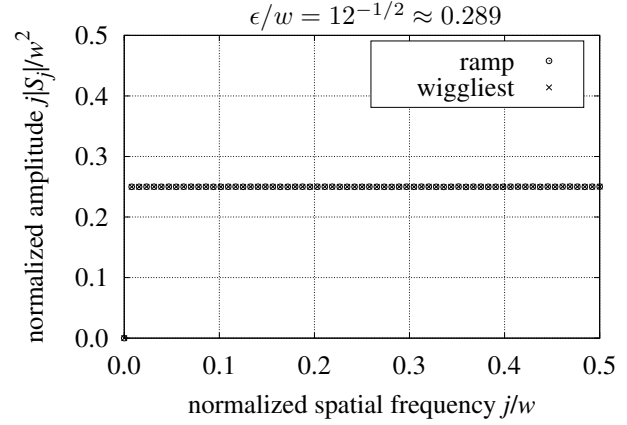


Figure 8 wiggliest and ramp spectra

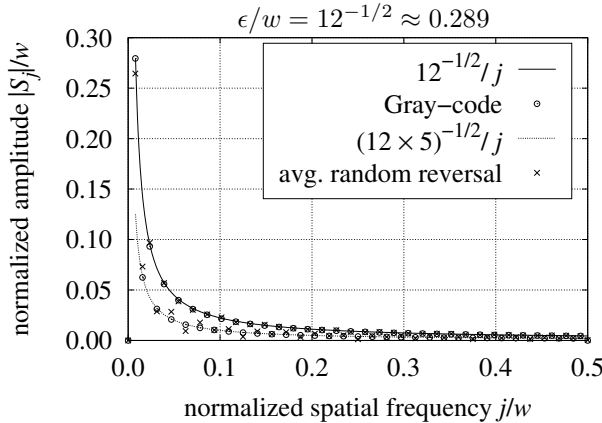


Figure 9 Gray and random spectra

Figure 9 shows the $|S_j|/w$ spectrum of the Gray-code roughness profile (Figure 1), and the averaged Fourier spectrum amplitudes from 187 instances of 128-point random reversal profiles. The similarity between these spectra indicates that Gray-code roughness is representative of self-similar ramp-permutation roughness. The Gray-code spectrum phases are evenly distributed among 0° , 180° , 63.43° , and 116.57° .

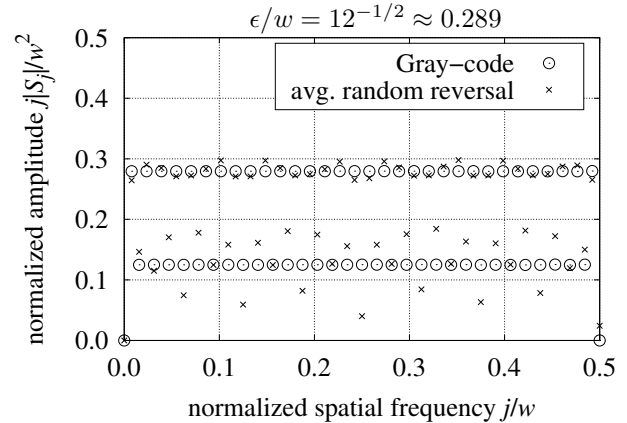


Figure 10 Gray and random spectra

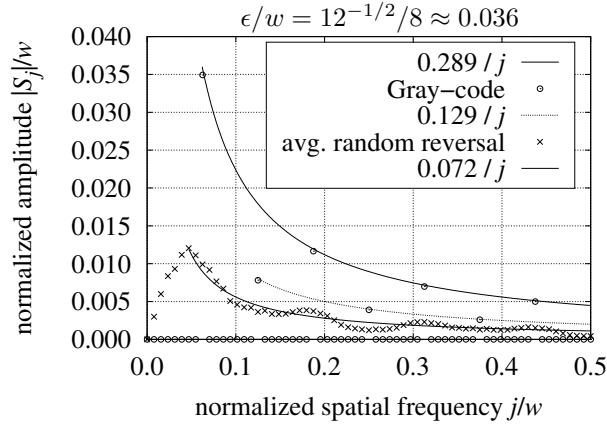


Figure 11 Gray and random eighths

Figure 11 shows the spectrum of eight concatenated repetitions of a Gray-code sequence, and the averaged Fourier spectrum amplitudes from 187 instances of eight concatenated random reversal sequences. The peak index j_P of Gray-code eighths is 8, as expected, but the random reversal sequences have $j_P = 6$ because the amplitudes aren't correlated between the random eighths.

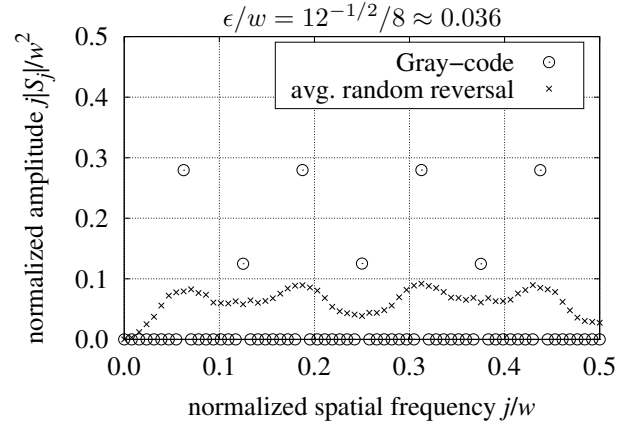


Figure 12 Gray and random eighths

Self-similar roughness amplitudes scale as w/j . In order to reveal the spectral structure of roughness across scale, $j|S_j|/w^2$ normalizes the spectrum relative to the ramp spectrum. Figures 8, 10, and 12 show $j|S_j|/w^2$ spectra corresponding to the $|S_j|/w$ spectra in Figures 7, 9, and 11, respectively. Amplitudes repeating across the spatial frequencies indicates self-similarity.

Top level self-similar roughness has $j_P = 1$; $j_P \gg 1$ indicates periodic roughness, whether subsections are self-similar or not.

9. Periodic roughness

The concept of “uniform roughness” is incompatible with self-similarity; the RMS height-of-roughness of a portion of a self-similar surface must shrink with the succession of scales converging to 0.

Let a plate with “periodic roughness” be a weakly isotropic array of many co-planar, uniformly sized patches, each having the same RMS height-of-roughness ε . Each patch is independently self-similar or not.

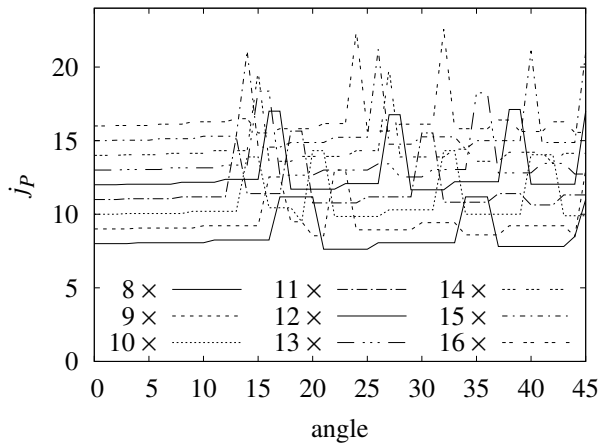


Figure 13 bi-level plate j_P versus angle

The effective period $L_P = L/\sqrt{j^2 + k^2}$, where j, k are the indexes of the 2-dimensional discrete spatial Fourier transform coefficient $X_{j,k}$ with the largest amplitude. Figure 13 shows $j_P = \sqrt{j^2 + k^2}$ for a square equal-area bi-level surface (regular array of square posts on flat plate) computing $X_{j,k}$ from a 64×64 sampling of that surface at flow angles from 0° through 45° at scales $8\times$ to $16\times$. At each scale, j_P varies within a 1.5 : 1 range versus angle. This suggests a quantitative criterion for weak isotropy:

A surface is weakly isotropic if its effective period L_P varies less than 1.5 : 1 through a full rotation.

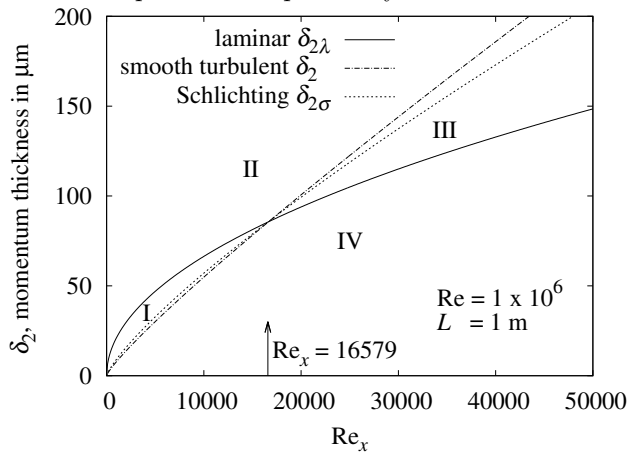


Figure 14 smooth plate δ_2 versus Re_x

Described in Section 1, both sand-roughness and the sphere-roughened (Pimenta et al) plate were periodic roughnesses because both the sand grains and metal spheres had uniform size and spacing.

For a periodic roughness with $0 < \varepsilon < L_P \ll L$ there must be some value of $\text{Re} > 0$ below which the flow exhibits laminar or smooth turbulent behavior along the entire plate. The boundary layer is thinnest at the leading edge. If the boundary layer is going to be disrupted, then it will start within the leading band ($0 < x < L_P$) of periodic roughness. In the present analysis, a boundary layer is considered disrupted when $2\varepsilon > \delta_2(L_P)$, where $\delta_2(x)$ is the boundary-layer momentum thickness at x .

$\delta_2(x)$ is the thickness of bulk flow having the same momentum flow rate (per unit plate area) as the plate boundary layer at x . Momentum thickness δ_2 isn't a directly measurable quantity. Schlichting [6] gives the momentum thickness of laminar and smooth turbulent boundary layers as $\delta_{2\lambda}(x) = 0.664 x \text{Re}_x^{-1/2}$ and $\delta_{2\sigma}(x) = 0.036 x \text{Re}_x^{-1/5}$, respectively. The local Reynolds number $\text{Re}_x = \text{Re} x/L$. Equivalently, the laminar and smooth turbulent boundary-layer thicknesses are:

$$\delta_{2\lambda}(x) = 0.664 \sqrt{\text{Re}_x} \frac{L}{\text{Re}} \quad \delta_{2\sigma}(x) = 0.036 \text{Re}_x^{4/5} \frac{L}{\text{Re}} \quad (32)$$

The laminar flow $\delta_{2\lambda}$ is from the Blasius boundary-layer model, which is well supported by measurement. The smooth turbulent $\delta_{2\sigma}$ formula is less certain. Continuing the analysis of smooth turbulent skin-friction, with free variable ε , let L/ε be the value producing the rough-to-smooth turbulence transition at local Reynolds number Re_x . Solving formula (26) for L/ε :

$$\frac{L}{\varepsilon} = \exp\left(W_0\left(\frac{\text{Re}_x}{\sqrt{3}}\right)\right) \quad (33)$$

The momentum thickness $\delta_2(x)$ should be proportional to the product of x (the distance from the leading edge) and the ratio of the friction velocity v^* from formula (23) to the bulk flow velocity v :

$$\delta_2(x) \propto x \frac{v^*}{v} = \frac{x}{\sqrt{3} \ln(L/\varepsilon)} = \frac{x}{\sqrt{3} W_0(\text{Re}_x/\sqrt{3})} \quad (34)$$

The coefficient seems to be $1/3^3 = 1/27 \approx 0.0370$, which may be related to $\exp(\varphi \ln(\varphi)) \equiv \varphi^\varphi$.

$$\delta_2(x) = \frac{x}{3^3 W_0(\text{Re}_x/\sqrt{3})} \quad \text{Re}_x > \sqrt{3}e \quad (35)$$

Figure 14 demonstrates that "smooth turbulent" δ_2 from equation (35) and $\delta_{2\sigma}$ from equation (32) are close to each other between the origin and the intersection of the laminar and turbulent curves at:

$$0.664 \sqrt{\text{Re}_x} = 0.036 \text{Re}_x^{4/5} \quad \text{Re}_x = \left[\frac{0.664}{0.036}\right]^{10/3} \approx 16579 \quad (36)$$

Because $L_P \ll L$, when $x = L_P$, then $\text{Re}_x \ll \text{Re}$; hence, $\delta_{2\sigma}(L_P)$ is a reasonable approximation for $\delta_2(L_P)$ in the leading band of roughness.

Figure 14 shows the theoretical momentum thickness of laminar and smooth turbulent flows along a 1 m long plate with $\text{Re} = 1 \times 10^6$. The laminar and turbulent curves divide the graph into four regions. When the point at coordinates $[\text{Re}_x, 2\varepsilon]$ is in regions I or IV, then it won't significantly disrupt laminar flow; hence, the flow along the plate will be laminar. When $[\text{Re}_x, 2\varepsilon]$ is in region II, then its height is sufficient to disrupt both laminar and smooth turbulent flow; so the flow along the plate will be rough turbulent.

When $[\text{Re}_x, 2\varepsilon]$ is in region III, then the roughness is sufficient to disrupt laminar flow, but not large enough to disrupt smooth turbulent flow; so the flow along the plate will be smooth turbulent. With $\delta_{2\lambda} = 2\varepsilon = \delta_{2\sigma}$ and $x = L_P$, solve for laminar upper-bound Re_λ and smooth turbulent upper-bound Re_σ :

$$\text{Re}_\lambda = \left[\frac{0.664}{2\varepsilon}\right]^2 L_P L \quad (37)$$

$$\text{Re}_\sigma = \left[\frac{0.036}{2\varepsilon}\right]^5 L_P^4 L \quad (38)$$

Equating Re_λ and Re_σ yields their intercept:

$$\frac{L_P}{\varepsilon} = \left[\frac{0.332^2}{0.018^5} \right]^{1/3} \approx 387.8 \quad (39)$$

When $L_P/\varepsilon < 387$, then $\text{Re}_\sigma < \text{Re}_\lambda$ and the flow along the entire plate transitions directly from laminar to rough turbulence at $\text{Re} \approx \text{Re}_\lambda$. When $L_P/\varepsilon > 388$, then $\text{Re}_\sigma > \text{Re}_\lambda$ and the flow along the entire plate transitions from laminar to smooth turbulence at $\text{Re} \approx \text{Re}_\lambda$, and to rough turbulence at $\text{Re} \approx \text{Re}_\sigma$.

Lienhard [15] models a gradual transition from laminar to smooth turbulence for smooth plates. In contrast, for periodic roughness $L_P \ll L$ and $\text{Re}_x \ll \text{Re}$; thus, the transition will be abrupt because it takes place in the leading band of roughness.

10. Periodic smoothness

In the discussion appended to Hama [3], Dr. S. F. Hoerner points out:

“... there is hardly any physical or natural surface condition which is truly equal or similar to sand roughness. One conclusion from sand experiments has been the expectation that from then on every rough surface should have a constant terminal drag coefficient. As early as 1924, it has been demonstrated (by Hopf and Fromm in *Zeitschr. Angew. Math. Mech.*, 1923:329-339) that certain types of roughness do not show any constant coefficients.”

Consider a smooth flat plate etched with a square grid of grooves subjected to a moderate flow parallel to its surface. When the boundary layer is disrupted by a groove perpendicular to the flow, the smooth turbulent boundary layer restarts at the edge of the flat patch. At the scale of the roughness period L_P , the momentum thickness of the boundary layer grows from 0 to the $\delta_2(x)$ value from the plate at L -scale.

For a given RMS height-of-roughness ε , the larger the portion of the L_P band that the flat occupies, the deeper the grooves must be in order to have overall height-of-roughness ε . For a bi-level plate of peak-to-valley height ε_{pv} having L_T -square posts in L_P -square cells:

$$\bar{z} = \frac{L_T^2 \varepsilon_{pv}}{L_P^2} \quad \varepsilon = \sqrt{(\varepsilon_{pv} - \bar{z})^2 \frac{L_T^2}{L_P^2} + \bar{z}^2 \left[1 - \frac{L_T^2}{L_P^2} \right]} = \frac{1}{L_P} \sqrt{(\varepsilon_{pv} - \bar{z})^2 L_T^2 + \bar{z}^2 [L_P^2 - L_T^2]} \quad (40)$$

Given L_T , L_P , and ε , what is the height ε_{pv} between the two levels?

$$\varepsilon_{pv} = \frac{\varepsilon L_P^2}{L_T \sqrt{L_P^2 - L_T^2}} \geq 2\varepsilon \quad (41)$$

If the smooth turbulent momentum thickness grows to exceed ε_{pv} , then the rest of the plate (to its trailing edge) will have smooth turbulent skin-friction coefficient $f_{C\sigma}$. Equating ε_{pv} and $\delta_{2\sigma}$:

$$\varepsilon_{pv} = 0.036 x^{4/5} \left[\frac{L}{\text{Re}} \right]^{1/5} \quad \frac{\varepsilon_{pv} \text{Re}}{L} = 0.036 \left[\frac{x \text{Re}}{L} \right]^{4/5} \quad \text{Re}_x = \left[\frac{\text{Re} \varepsilon_{pv}}{0.036 L} \right]^{5/4} \quad (42)$$

There are considerations in addition to $\varepsilon_{pv} < \delta_{2\sigma}$ for determining where the flow will transition to smooth turbulence. If ε_{pv} is large while the gap is small, then the flow will transition to smooth turbulence at smaller x and Re_x values than it would otherwise. Formula (43) introduces three dimensionless factors to reduce the rough turbulence upper-bound Re_ℓ as the flat length L_T , effective gap width $\sqrt{L_P^2 - L_T^2}$, or ε_{pv} shrinks. The $[L/(\text{Re} L_P)]^{5/4}$ factor normalizes Re_x at plate-scale L to Re at scale L_P . The L/L_P factor converts the characteristic-length from L_P back to L . Flow transitions from rough to smooth turbulence where $\text{Re}_x \approx \text{Re}_\ell$.

$$\begin{aligned} \text{Re}_\ell &= \frac{\sqrt{L_P^2 - L_T^2}}{0.036 L_P} \frac{\varepsilon_{pv}/4}{\sqrt{L_P^2 - L_T^2}} \frac{L_T}{0.036 L_P} \frac{L}{L_P} \left[\frac{L}{\text{Re} L_P} \right]^{5/4} \left[\frac{\text{Re} \varepsilon_{pv}}{0.036 L} \right]^{5/4} \\ &= \frac{L L_T \varepsilon_{pv}/4}{0.036^2 L_P^3} \left[\frac{\varepsilon_{pv}}{0.036 L_P} \right]^{5/4} = \frac{L L_T/4}{0.036 L_P^2} \left[\frac{\varepsilon L_P}{0.036 L_T \sqrt{L_P^2 - L_T^2}} \right]^{9/4} \quad \frac{1}{2} \leq \frac{L_T^2}{L_P^2} < 1 \end{aligned} \quad (43)$$

Formula (43) should be roughly indicative for other periodic, weakly isotropic grooved plates whose flats have convex perimeters. Use square-root of the flat area as L_T and square-root of the cell area as L_P .

11. Local skin-friction

Conversions between local and average skin-friction are needed in order to compare prior with present work.

The ratio of average to local skin-friction $f_C/f_c > 1$ of a continuous boundary layer is calculated from local skin-friction coefficient f_c by formula (44). The singularity at the leading edge of the plate is avoided by using $\text{Re}_0 > 0$ as the integration lower bound; Re_0 must be chosen such that $f_c(\text{Re}_0) \ll 1$.

$$\frac{f_C(\text{Re})}{f_c(\text{Re})} = \frac{1}{\text{Re} - \text{Re}_0} \int_{\text{Re}_0}^{\text{Re}} \frac{f_c(\text{Re}_x)}{f_c(\text{Re})} d\text{Re}_x \quad (44)$$

The local skin-friction coefficient f_c isn't well-defined for self-similar roughness because its L/ε is constant. Periodic roughness has varying L/ε ; it also provides L_P/ε as the lower bound of integration.

A crucial difference between periodic roughness and smooth surfaces is that periodic roughness disrupts the boundary layer repeatedly. Thus, the local skin-friction coefficients being averaged are independent; instead of f_C/f_c accruing linearly, it should go as the square:

$$\frac{f_C(L/\varepsilon)}{f_c(L/\varepsilon)} = \left[\frac{\varepsilon}{L - L_P} \int_{L_P/\varepsilon}^{L/\varepsilon} \frac{f_c(r)}{f_c(L/\varepsilon)} dr \right]^2 \quad (45)$$

Applying formula (45) to the Mills-Hang local formula (5) yields the average skin-friction coefficient:

$$C_D^2 / C_f \quad (46)$$

where C_f and C_D are from equations (5) and (6), respectively.

At $L/\varepsilon = 4000$ ($L/k_S = 750$), formula (46) has values in excess of 20% larger than the Mills-Hang C_D formula (6) derived using averaging formula (9). The average skin-friction coefficient was of minor importance in Mills and Hang [5], and wasn't compared with measurements of average skin-friction.

For a disrupted boundary layer, the transform for local friction f_c given average friction f_C is:

$$\frac{f_c(L/\varepsilon)}{f_C(L/\varepsilon)} = \left[\frac{d([L - L_P] f_C(L/\varepsilon))}{dL} / f_C(L/\varepsilon) \right]^2 \quad (47)$$

Applying formula (47) to average formula (24) for rough surfaces yields the local skin-friction coefficient:

$$f_c(x/\varepsilon) = \frac{1}{3} \left[\frac{\ln(x/\varepsilon) + 2 [L_P/x - 1]}{\ln^2(x/\varepsilon)} \right]^2 \quad L \geq x > L_P \geq \varepsilon \quad (48)$$

The local skin-friction coefficient for smooth turbulent flow can be derived from equations (28) and (49) with $\text{Re}_x \geq \text{Re}_0 \geq \sqrt{3}e$ and $\text{Re}_x \gg \sqrt{3}e$:

$$\frac{dW_0(\vartheta)}{d\vartheta} = \frac{W_0(\vartheta)}{\vartheta [W_0(\vartheta) + 1]} \quad f_{c\sigma}(\text{Re}_x) = \frac{d([\text{Re}_x - \text{Re}_0] f_{C\sigma}(\text{Re}_x))}{d\text{Re}_x} \quad (49)$$

$$f_{c\sigma}(\text{Re}_x) = \frac{\sqrt[3]{2} W_0^2(\text{Re}_x/\sqrt{3}) - 2 [1 - \text{Re}_0/\text{Re}_x] W_0(\text{Re}_x/\sqrt{3}) - 1}{3 [W_0(\text{Re}_x/\sqrt{3}) - 1]^3 [W_0(\text{Re}_x/\sqrt{3}) + 1]} \quad (50)$$

Local smooth turbulent skin-friction coefficient formulas and data values provided by Churchill [8] are shown in Figure 15. The ‘‘present work’’ formula (50) has 2% RMS relative error (RMSRE) from the ‘‘Smith-Walker and Spalding-Chi measurements’’.

Note that when calculating RMSRE, the increase from a variation at a single point is larger than the increase when that variation is split among multiple points. Thus, local measurements tend to have larger RMSRE than average measurements. In Figure 15, the primary error contributor is the value at $\text{Re}_x = 10^7$.

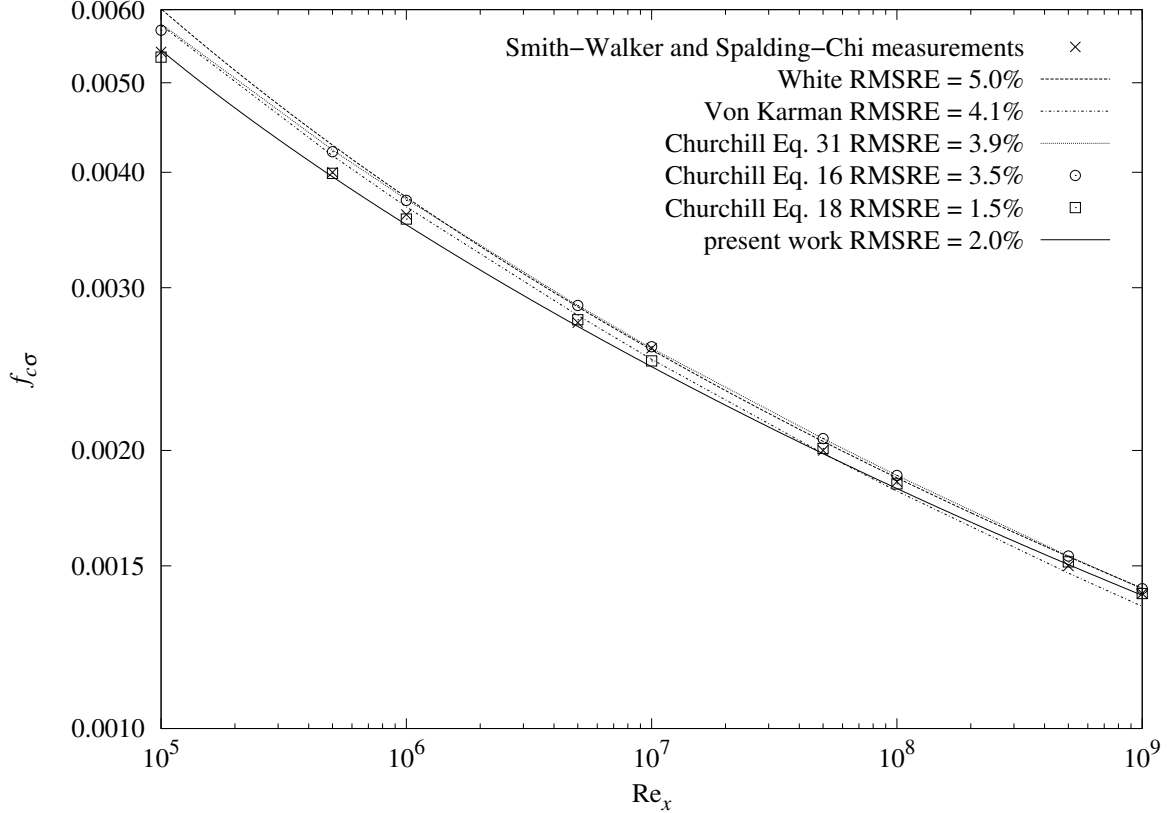


Figure 15 local $f_{c\sigma}$ versus Re_x of smooth plate

12. Forced convection

Forced convective heat transfer is expressed as the dimensionless average (\overline{Nu}) or local (Nu) Nusselt number. Heat transfer by rough turbulence will grow with the amount of turbulence induced, $f_C Re$. It will also grow with the fluid's Prandtl number (Pr), the ratio of kinetic viscosity to thermal diffusivity. Fluids with large Pr transport heat in the fluid flow; conduction is dominant in fluids with small Pr . The $1/3$ exponent for Pr may relate to it being a property of the fluid in three dimensions. Heat transfer from the trailing part of the plate is reduced due to fluid heating by the leading part; hence, formula (51) is scaled by $1/2$. Expanding f_C from equation (24) yields formula (51) for rough turbulent average forced convection:

$$\overline{Nu} = \frac{f_C Re Pr^{1/3}}{2} = \frac{Re Pr^{1/3}}{6 \ln^2(L/\varepsilon)} \quad \frac{L}{\varepsilon} \gg 1 \quad Pr > 0 \quad (51)$$

The analysis for self-similar f_C didn't involve boundary layers; hence, there is no restriction to $Pr > 0.6$. The Colburn [16] analogies relate friction factors to forced convective heat transfer. For laminar flow:

$$\overline{Nu} = \frac{f_C}{2} Re Pr^{1/3} \quad (52)$$

Note that equation (51) also results from combining equation (52) with f_C equation (24).

For smooth turbulent convection, Lienhard [15] recommends composing the Gnielinski formula (53) with the White skin-friction formula (8). Note that formula (53) is local convection (Nu).

$$Nu = \frac{Re_x Pr C_f/2}{1 + 12.7 [Pr^{2/3} - 1] \sqrt{C_f/2}} \quad Pr \geq 0.6 \quad (53)$$

Lienhard states that formula (54) has similar accuracy for gases:

$$Nu = 0.0296 Re_x^{4/5} Pr^{0.6} \quad \overline{Nu} = 0.037 Re^{4/5} Pr^{0.6} \quad (54)$$

Equation (28) is an exact formula for skin-friction; can an exact forced convection formula be derived?

Jaffer [17] derives exact natural convection formulas. Natural convection from a vertical plate is similar to forced convection; in both, the flow is uniform along the plate's characteristic-length L .

Jaffer finds that stationary fluid conducts heat from the plate with an effective Nusselt number Nu_0 :

$$Nu_0 = \frac{16}{\pi^2 \sqrt[4]{2}} \approx 1.364 \quad (55)$$

The flow-induced heat transfer will grow with $Nu_0 \text{Re} f_{C\sigma}$. Because heat must traverse boundary layers, the smooth convection dependence on Pr is more complicated than $\text{Pr}^{1/3}$. The vertical-plate natural convection \overline{Nu} dependence on Pr is $\sqrt[3]{\text{Pr}/\Xi}$, where $\Xi(\text{Pr})$ is defined using the ℓ^p -norm with $p = \sqrt{1/3}$:

$$\Xi(\text{Pr}) = \left\| 1, \frac{0.5}{\text{Pr}} \right\|_{\sqrt{1/3}} \quad \|\varphi, \vartheta\|_p = (|\varphi|^p + |\vartheta|^p)^{1/p} \quad (56)$$

Figure 16 shows that $\sqrt[3]{\text{Pr}/\Xi}$ is asymptotically $\sqrt[3]{\text{Pr}}$ for large Pr and $\sqrt[3]{2}\text{Pr}^{2/3}$ for small Pr . At small Pr , conduction doesn't amplify forced convection as it does natural convection; the Pr exponent should be 1. An additional factor using the ℓ^3 -norm accomplishes this. Formula (57) is asymptotically $\sqrt[3]{2}\text{Pr}$ at $\text{Pr} < 0.5$. The “ $0.7\text{Pr}^{0.6}$ ” trace shows that formula (57) has a slope close to formula (54) for gases.

$$\sqrt[3]{\frac{\text{Pr}}{\Xi}} \sqrt[3]{\frac{1}{\|1, 1/\text{Pr}\|_3}} \quad (57)$$

The slope of formula (53) $Nu(\text{Re}_x)$ decreases with increasing Pr ; for large Pr , $Nu \propto \sqrt{C_f}$. Recall from equations (22) and (23) that $\sqrt{f_C}$ is proportional to friction velocity v_* ; this indicates that transport through the boundary layer limits convection at large Pr . In order to reduce asymptotic dependence from $f_{C\sigma}$ to $\sqrt{f_{C\sigma}}$, convection will include a factor taking square-root of an expression gating $1/f_{C\sigma}$ by Pr :

$$\sqrt{\frac{\text{Pr}/9 + 1}{18 f_{C\sigma} \text{Pr} + 1}} \quad (58)$$

The scaling for upstream heating was $1/2$ in formula (51) for disruptive roughness; the smooth turbulent boundary layer reduces this interaction; $\sqrt{1/3} \approx 0.577$ appears correct in the smooth case.

Formula (59) is proposed for smooth-turbulent convection for all $\text{Pr} > 0$:

$$\overline{Nu}_\sigma = \frac{Nu_0 \text{Re} f_{C\sigma}}{\sqrt{3}} \sqrt{\frac{\text{Pr}/9 + 1}{18 f_{C\sigma} \text{Pr} + 1}} \sqrt[3]{\frac{\text{Pr}}{\Xi \|1, 1/\text{Pr}\|_3}} \quad \text{Re} \gg \sqrt{3} e \quad (59)$$

Lienhard [15] compares the Gnielinski-White convection formula with local measurements from studies of a variety of fluids with $0.7 \leq \text{Pr} \leq 257$ spanning $4000 < \text{Re}_x < 4.3 \times 10^6$. The smallest turbulent Re_x presented was $\approx 10^5$. Note that formula (54) is more accurate than Gnielinski-White for turbulent air ($\text{Pr} \approx 0.71$) at $\text{Re}_x < 10^5$.

Figures 17 and 18 show \overline{Nu} versus Pr and Re . The “present work” traces are formula (59). The “Lienhard” traces use formula (60) to numerically average the composition of Gnielinski formula (53) with White formula (8). Note that the averaging of convection $Nu(\text{Re}_x)$ in formula (60) is different from the averaging of skin-friction coefficients presented in Section 11.

$$\overline{Nu}(\text{Re}) = \int_{\text{Re}_0}^{\text{Re}} \frac{Nu(\text{Re}_x)}{\text{Re}_x} d\text{Re}_x \quad (60)$$

Formula (59) \overline{Nu}_σ matches the numerically averaged Gnielinski-White formula within $\pm 6.5\%$ over the range $10^5 < \text{Re} < 4.3 \times 10^6$ with $4.0 \leq \text{Pr} \leq 257$. At $\text{Pr} = 0.71$, \overline{Nu}_σ matches formula (54) \overline{Nu} within $\pm 4\%$ over the range $10^4 < \text{Re} < 4.3 \times 10^6$.

Over the same ranges, the local convection $Nu_\sigma = \text{Re}_x d\overline{Nu}_\sigma(\text{Re}_x)/d\text{Re}_x$ matches formula (53) and local formula (54) Nu within $\pm 7.5\%$. Figure 19 shows local Nu versus Re_x .

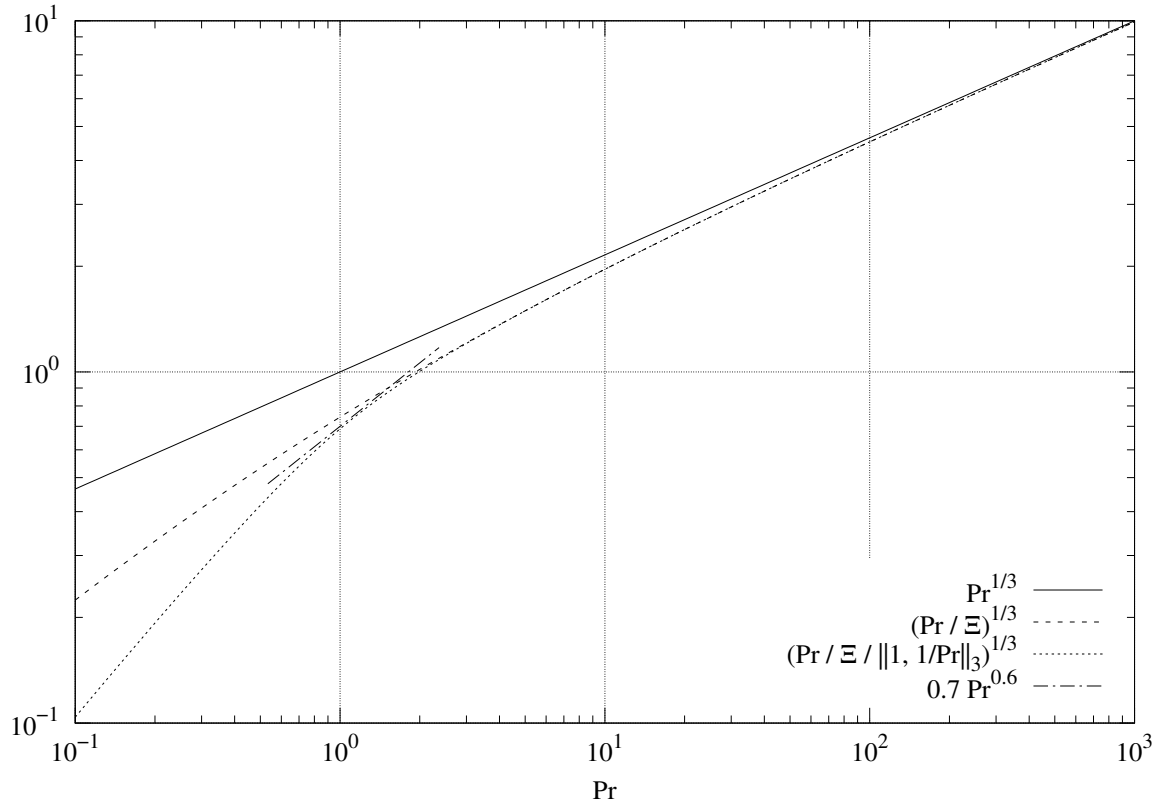


Figure 16 smooth plate \overline{Nu} dependence on Pr

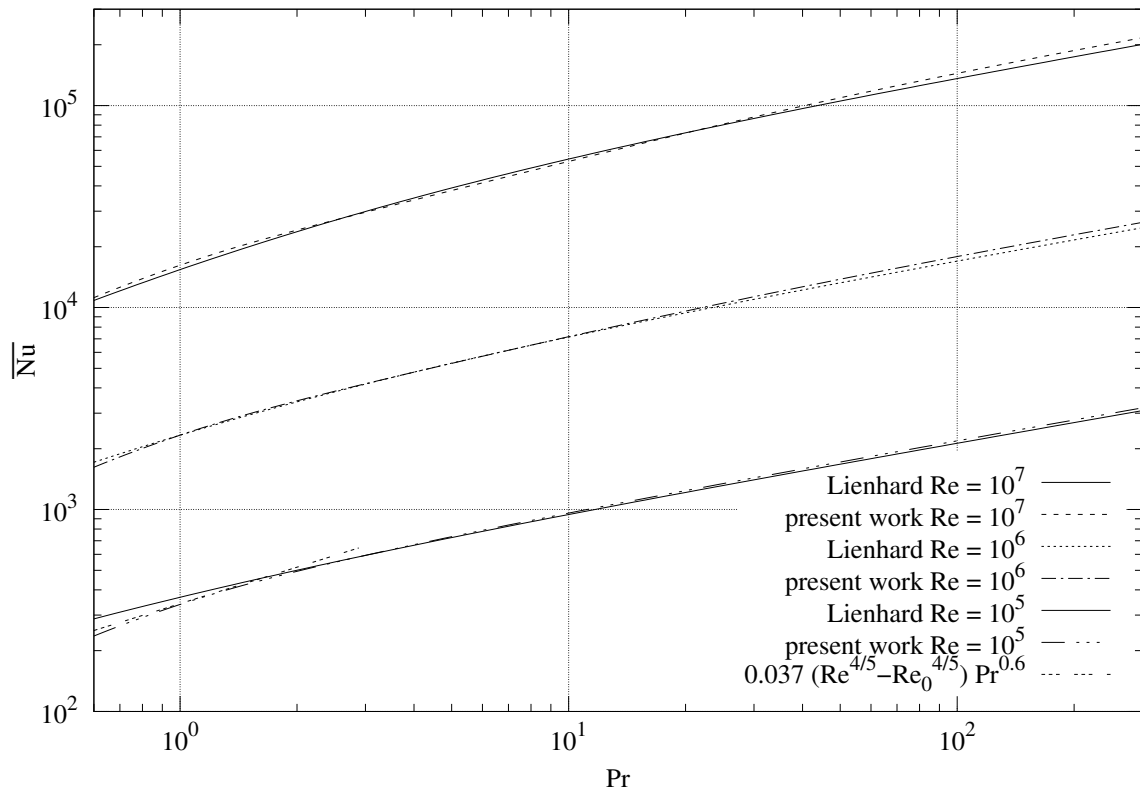


Figure 17 smooth plate average turbulent convection versus Pr

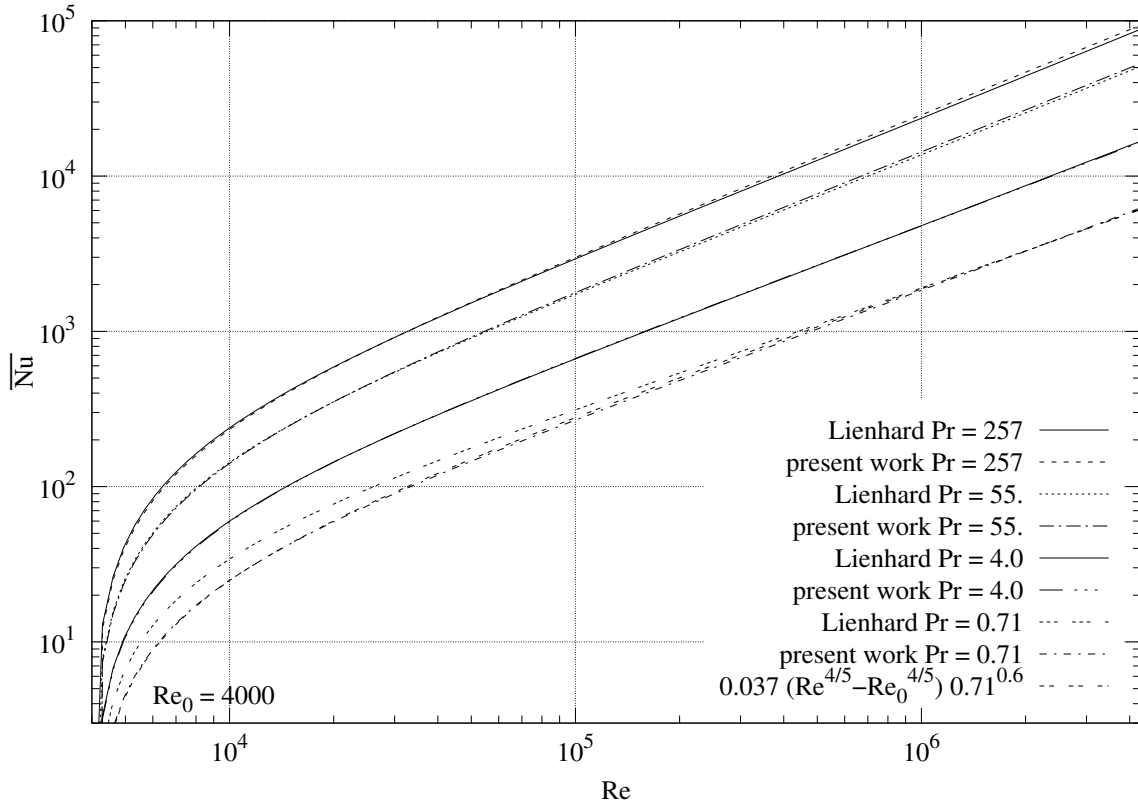


Figure 18 smooth plate average turbulent convection versus Re

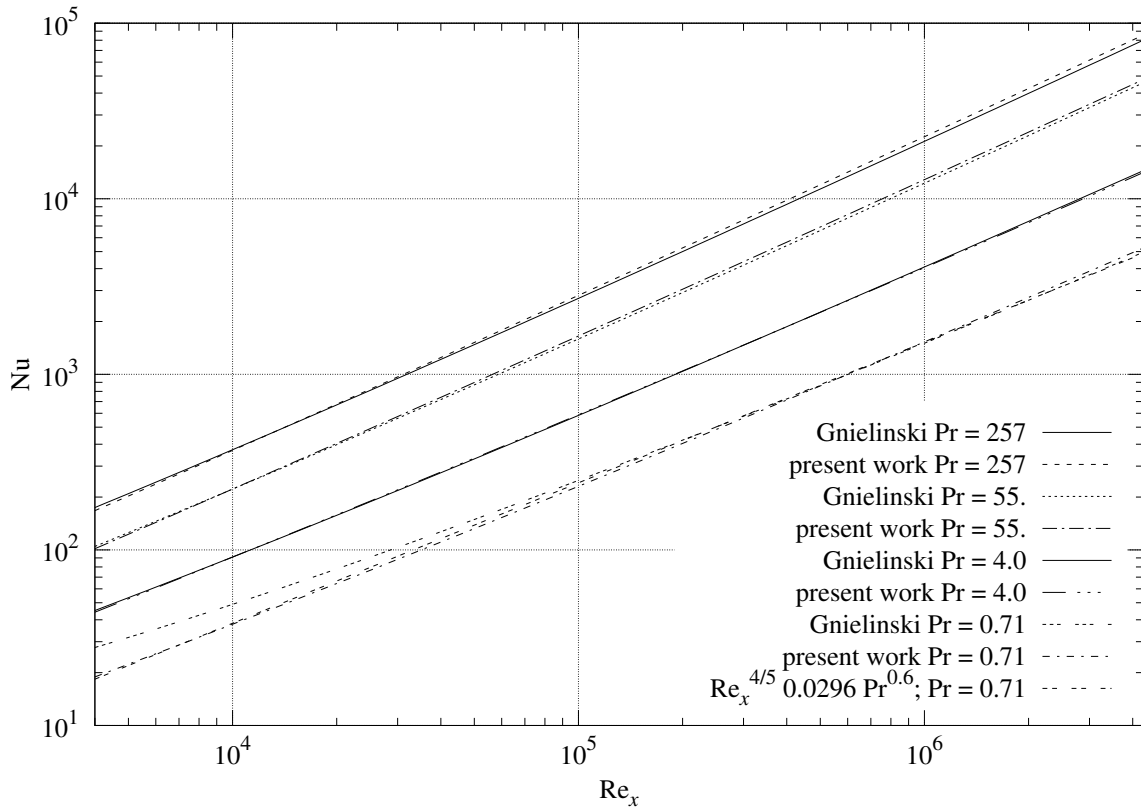


Figure 19 smooth plate local turbulent convection versus Re_x

13. Periodic versus self-similar roughness

What can be learned from measurements of skin-friction coefficient and forced-convection from rough plates?

The skin-friction and convection formulas were developed for self-similar roughness. If measurements of plates with self-similar roughness are close to the predictions of skin-friction equation (24) or convection equation (51), then those measurements support the present formulas for self-similar roughness only.

If measurements over a range of Re values from diverse plates with periodic roughness are close to the present formulas, then it's evidence that the present formulas reflect a physical law of turbulent flow along surface roughness. Only periodic roughness was tested in the present and prior works.

14. Fully rough regime

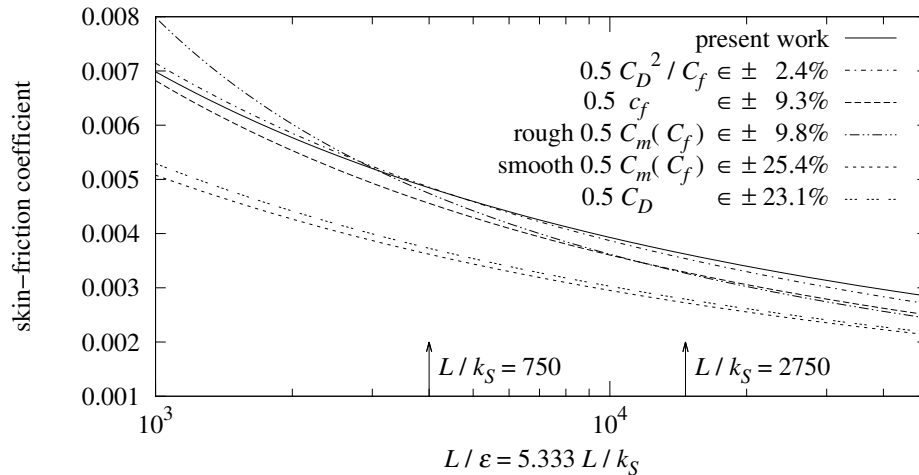


Figure 20 average friction coefficient of sand-roughness

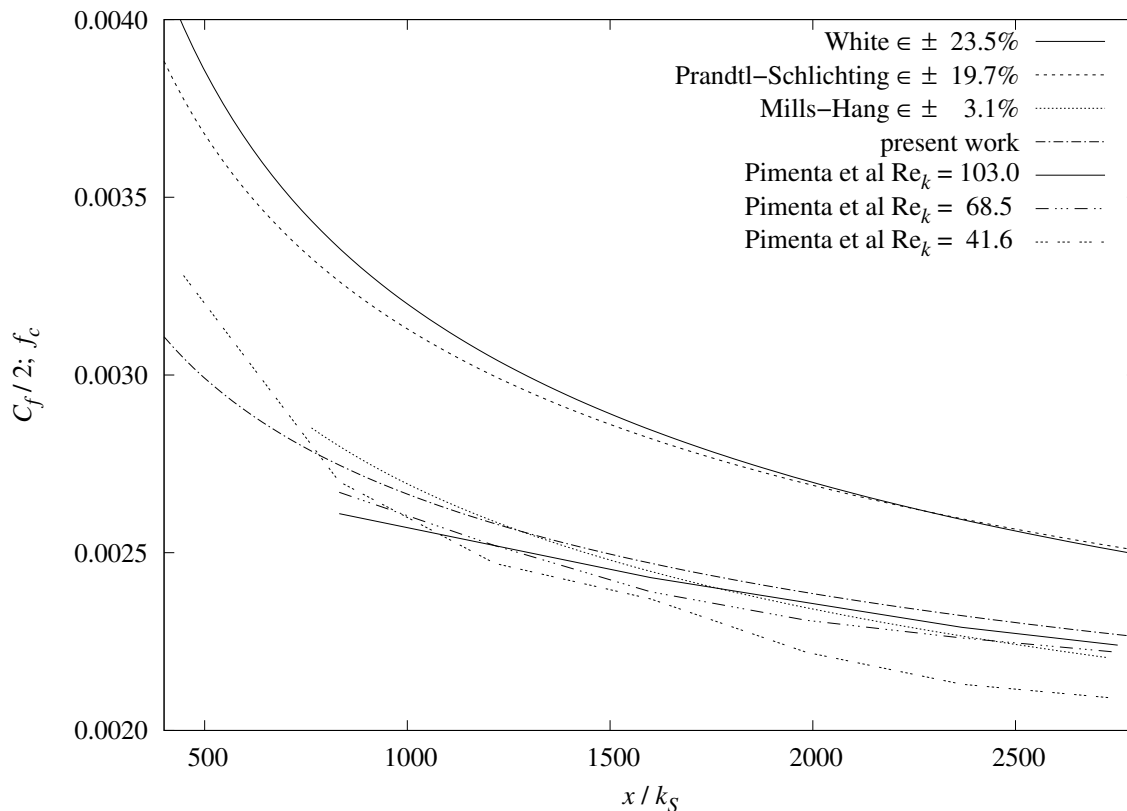


Figure 21 local friction coefficient of sphere-roughened plate

Figure 20 compares average skin-friction formulas in the fully rough regime. To the right of each “ $\in \pm$ ” is the maximum discrepancy from “present work” equation (24) over the Mills-Hang range $750 < L/k_S < 2750$.

Starting from the bottom of the Figure 20 key, “0.5 C_D ” is the Mills-Hang average formula (6).

The two “0.5 $C_m(C_f)$ ” traces are the Churchill smooth and rough averaging formulas (10) applied to the Mills-Hang local formula (5).

“0.5 c_f ” is the Prandtl-Schlichting average formula (4).

“0.5 C_D^2/C_f ” is the disrupted boundary-layer averaging formula (46) applied to the Mills-Hang local formula (5); it’s within $\pm 2.4\%$ of the present work equation (24).

Figure 21 plots the local skin-friction coefficients from White (7), Prandtl-Schlichting (3), Mills-Hang (5), and the present theory (48) in the fully rough regime (large Re). The maximum magnitude discrepancy between Mills-Hang and the present theory is 3.1% over the Mills-Hang range $750 < x/k_S < 2750$.

The close matches in the fully rough regime, both average and local, support the present theory with measurements from Pimenta et al [4] as modeled by Mills and Hang [5].

15. Transitional rough regime

Prandtl and Schlichting describe the boundaries between flow regimes using the “sand-roughness Reynolds number” $Re_k = v^* k_S / \nu \approx 5.333 Re_\varepsilon$ (Re_ε from present work equation (25)). They assign the boundaries between the hydraulically smooth, transitional rough, and fully rough regimes at $Re_k = 7.08$ and 70.8 .

Afzal et al [9] (also Schlichting [6]) relates that the turbulent flow inside commercial pipes behaves differently from the flow inside Nikuradse’s sand coated pipes in the transitional rough regime. While the skin-friction coefficients for commercial pipes are monotonically decreasing with increasing Re on the Moody diagram (f_c versus Re), in the diagram for Nikuradse’s pipes the coefficient trace for each roughness reaches its minimum just to the right of the smooth skin-friction trace, a behavior termed “inflectional”.

The Prandtl-Schlichting plate model inherited the inflectional curve from Nikuradse’s pipes. The coefficients of resistance (c'_f and c_f) Moody diagrams from Prandtl and Schlichting [1, 6] show c'_f and c_f following a $-1/5$ slope smooth turbulent trace to a broad 7% dip to the right of the smooth turbulent trace, then rising and leveling out further to the right.

For periodic roughness, the present work’s local and average skin-friction formulas (48) and (24) predict no variation in these coefficients within the Re and Re_x range satisfying $\max(Re_\lambda, Re_\sigma) < Re$ and $Re_x < Re_\ell$.

The traces labeled “Pimenta et al” in Figure 21 show the local skin-friction coefficients versus x/k_S for the Pimenta et al sphere-roughened plate at three rates of flow, $Re_k = 41.6, 68.5,$ and 103 . The averages of these local coefficients from $750 < x/k_S < 2800$ are 0.00233, 0.00234, and 0.00241, respectively. These averages are within 3.4% of each other. The “Mills-Hang” trace is the fully rough local $C_f/2$; its close proximity to the “Pimenta et al” traces indicates a lack of significant behavioral difference between the fully rough and transitional rough regimes. This isn’t definitive, however, because $Re_k = 41.6$ is moderately close to the $Re_k = 65.0$ boundary that Pimenta et al assign between the transitional and fully rough regimes.

Figure 22 is a local Moody diagram showing Pimenta et al measurements at $x/k_S \approx 1200$, along with regime boundaries and skin-friction coefficients from Prandtl-Schlichting and the present work. The “asymptotic” trace at $c'_f \approx 0.006$ is the Prandtl-Schlichting fully rough skin-friction coefficient for $x/k_S = 1200$. The “monotonic” and “inflectional” traces are examples of those types of coefficients at $x/k_S = 1200$. The regime boundaries are in the positions expected for the “inflectional” trace.

The measured coefficients are less than half of the Prandtl-Schlichting c'_f coefficient for $x/k_S \approx 1200$. Both Mills-Hang and Pimenta et al take $c'_f/2$ (which they notate $C_f/2$) as the skin-friction coefficient. However, $Re \approx 1.2 \times 10^6$ (marked $Re_k \neq 65.0$) can’t be the transitional to fully rough boundary for $c'_f/2$ because it and the measurements are to the left of, and less than, the smooth turbulent trace $f_{c\sigma}$.

Nor can these measurements be of laminar flow. Laminar flow coefficients would have a larger magnitude slope (versus Re_x) than the smooth turbulent curve, but these measurements are nearly at the constant level predicted by the present work.

This is where the pipe-plate analogy fails. Rough turbulent skin-friction coefficients don’t take values less than the smooth turbulent skin-friction coefficient in pipes!

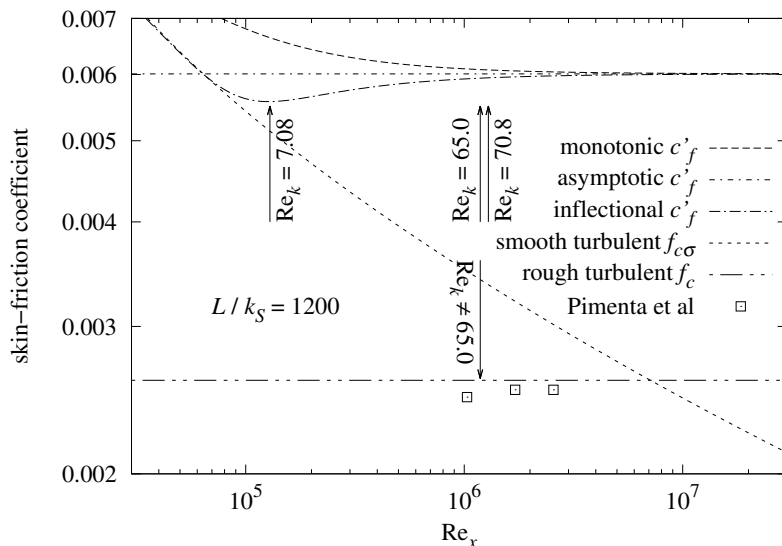


Figure 22 local c'_f versus Re_x

With $L_P/\varepsilon < 387$, formula (37) predicts that the flow along the entire sphere-roughened plate transitions directly from laminar to rough turbulence at $Re_\lambda \approx 6160$, but the smallest reported Re_x was 3.8×10^5 .

Figure 23 plots local f_c versus Re_x for the Pimenta et al data-set by Re_k . Except for the point at $[3.8 \times 10^5, 0.0033]$, the measurements are within $\pm 6\%$ of the present theory.

Note that all of these fully rough measurements are significantly less than “smooth turbulent $f_{c\sigma}$ ”.

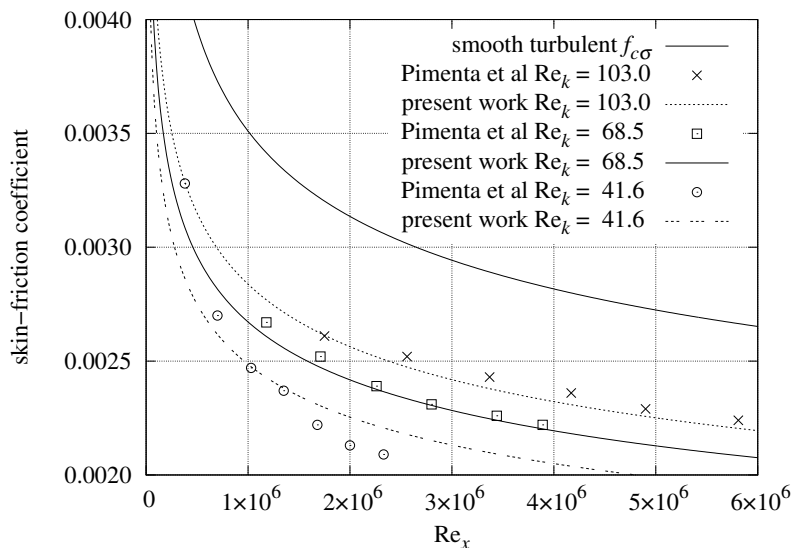


Figure 23 local f_c versus Re_x of sphere-roughened plate

16. Convection measurements

The present apparatus [18] combined an open intake wind-tunnel, a MIC-6 aluminum plate (with foam insulated backside) containing a heater, and transducers to measure temperature, pressure, and humidity. This combination was able to measure average convection in air at flow rates $2300 < Re < 90000$. The bi-level plate surface was milled to have (676) square $8.28 \text{ mm} \times 8.28 \text{ mm} \times 6 \text{ mm}$ posts spaced on 11.7 mm centers over the 0.305 m square plate. The area of the top of each post was 0.686 cm^2 , half of its 1.37 cm^2 cell. The RMS height-of-roughness and also the arithmetic-mean height-of-roughness were 3 mm . $L/\varepsilon \approx 102$, corresponding to $L/k_S \approx 19.1$. An equal-area bi-level architecture provides the largest RMS height-of-roughness (3 mm) possible in a given peak-to-valley span (6 mm). This surface was periodic, not self-similar. Figure 24 shows the plate suspended face down (to minimize the natural component of mixed convection) in the wind-tunnel.

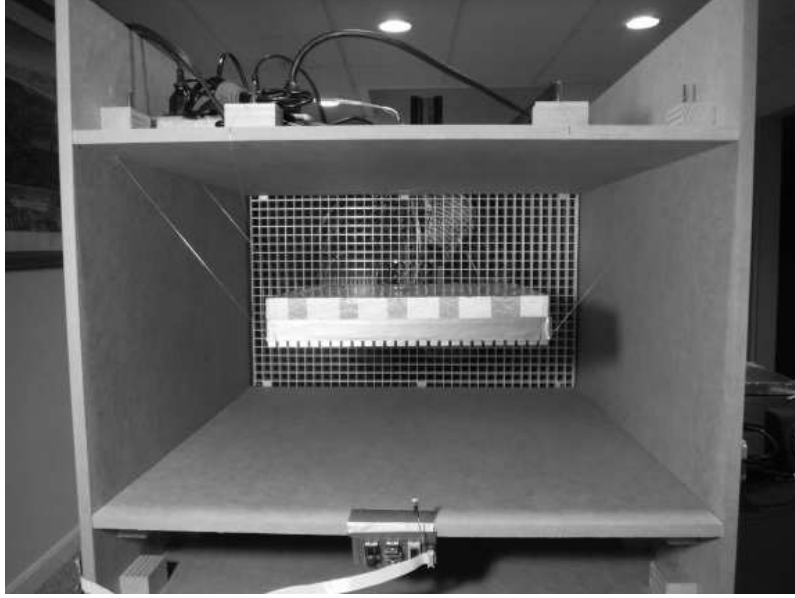


Figure 24 bi-level plate in wind-tunnel

The two sides of the plate roughness parallel to the flow also contribute to forced convection, increasing the effective width of the bi-level plate by $\sqrt{2}\varepsilon$ (1.4%). Applying the present convection formula (51) to the bi-level plate geometry (with the 1.4% correction) yields:

$$\overline{Nu} = 0.0079 \text{ Re Pr}^{1/3} \quad (61)$$

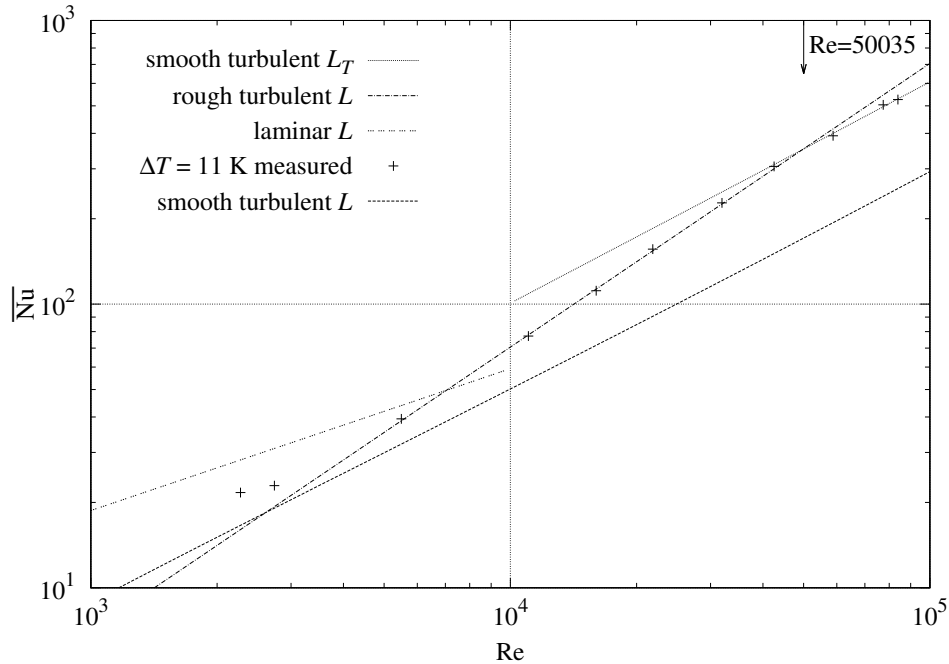


Figure 25 convection from bi-level plate; $L/\varepsilon = 305/3$

In Figure 25, the points labeled “ $\Delta T = 11$ K measured” are the \overline{Nu} values calculated from measurements with the plate 11 K warmer than the ambient air. At $\text{Re} < 5000$, the natural component dominates mixed convection. The “rough turbulent L ” trace in Figure 25 is equation (61); it matches the “measured” points $\pm 2.5\%$ for $5000 < \text{Re} < 50000$. At $\text{Re} > 50000$ the “smooth turbulent L_T ” trace (having slope $4/5$) shows that convection is from a smooth turbulent flow, but with a shorter characteristic-length than the “smooth turbulent L ” trace. Equation (43) calculates that this transition is at $\text{Re}_\ell \approx 50035$.

With $L_P/\varepsilon < 387$, formula (37) predicts that the flow along the entire bi-level plate transitions directly from laminar to rough turbulence at $\text{Re}_\lambda \approx 44$, which is too slow to test in the present apparatus.

The periodic bi-level plate behaving compatibly with formula (51), which was derived from an analysis of self-similar roughness, supports the claim that formulas (24) and (51) are intrinsic to turbulent flow along isotropic roughness, and not limited to self-similar roughness.

17. Discussion

Recapitulating the development:

- In rough turbulence, the surface roughness repeatedly disrupts emerging boundary layers along a plate.
- Self-similar roughness has a constant characteristic-length to RMS height-of-roughness ratio $L/\varepsilon \gg 1$ at a succession of scales converging to zero. This leads to friction velocity $v_* = v/[3 \ln(L/\varepsilon)]$.
- Plate surfaces with isotropic self-similar roughness have skin-friction coefficient: $f_C = [1/3] \ln^{-2}(L/\varepsilon)$.
- Consideration of $\text{Re}_\varepsilon = 1$ with free variable ε leads to an exact formula for the turbulent average skin-friction coefficient for smooth plates: $f_{C\sigma} = [\sqrt[3]{2}/3] [W_0(\text{Re}/\sqrt{3}) - 1]^{-2}$. This formula matches measurements from Smith and Walker [13] and Spalding and Chi [14] with 0.75% RMSRE.
- $j_P = \sqrt{j^2 + k^2}$, where j, k are the indexes of the Fourier transform coefficient $X_{j,k}$ with the largest amplitude. Self-similar roughness has $j_P = 1$; $j_P \gg 1$ is periodic roughness with period $L_P = L/j_P$.
- The transition from laminar or smooth turbulent flow to rough turbulent flow along a plate with isotropic periodic roughness should occur when 2ε exceeds the larger of the smooth turbulent or laminar momentum thicknesses of a smooth plate at $x = L_P$. Available data lacked Re small enough to verify the actual transitions. However, the data shows that the transitions must be at much smaller Re than the smooth-rough skin-friction intercept, which bounds the transition in pipes.
- Downstream from a disruption, a turbulent boundary layer restarts from zero thickness when along a flat, smooth patch. If this boundary layer grows large enough to bridge the rough bits outside of the smooth patches, then the flow downstream of Re_ℓ will be smooth turbulent.
- Converting between local and average skin-friction coefficients is different for flows having continuous versus disrupted boundary layers. Transforms in both directions were used to compare prior work local coefficients with present work average coefficients.
- Rough turbulent convection is: $\overline{\text{Nu}} = \text{Re Pr}^{1/3}/[6 \ln^2(L/\varepsilon)]$.
- The similarity of forced convection to natural convection from a vertical plate leads to a formula for smooth turbulent average forced convection. This formula matches the (averaged) turbulent formula from Lienhard [15] within $\pm 6.5\%$ over $10^5 < \text{Re} < 4.3 \times 10^6$ with $4.0 \leq \text{Pr} \leq 257$.
- Experiments with the periodic isotropic roughness of bi-level and sphere-roughened plates find that convection and skin-friction coefficients are close to the present theory's self-similar predictions with Re as small as 5000 and as large as 5×10^6 .
- Skin-friction and convection from such dissimilar rough surfaces hewing closely to the present theory is evidence that these formulas reflect physical laws of turbulent flow along isotropic surface roughness.

The RMS height-of-roughness to sand-roughness conversion factor (5.333) from Afzal et al [9] enabled prior work to be compared with the present work, matching Pimenta et al data and the Mills-Hang formula (5) to the present work within a few percent. When the sand-roughness to arithmetic-mean height-of-roughness conversion factor (6.45) from Afzal et al was tried, prior work significantly mismatched the present work.

The RMS height-of-roughness of ramp-permutations being $\varsigma/\sqrt{12}$ (versus $\varsigma/4$ for arithmetic-mean) is responsible for the appearance of threes in many coefficients of the present work's formulas.

Equating formula (24) f_C and formula (28) $f_{C\sigma}$ finds the average rough-smooth turbulence intercept:

$$\text{Re} = \sqrt{3} e \left[\frac{L}{\varepsilon} \right]^{\sqrt[6]{2}} \left[1 + \sqrt[6]{2} \ln \frac{L}{\varepsilon} \right] \quad \frac{L}{\varepsilon} \gg 1 \quad (62)$$

In the development of the Re_λ and Re_σ formulas, the comparison of δ_2 with 2ε is supported by the success of the Re_ℓ formula (43) applied to bi-level plates with $\varepsilon = 3$ mm and $\varepsilon = 1$ mm; Re_ℓ formula (43) compares $\delta_{2\sigma}$ with peak-to-valley height ε_{pv} , and ε_{pv} is never smaller than 2ε .

Equation (52) is the original (1933) form of the Chilton-Colburn analogy. Lienhard [15] demonstrates that the analogy's Re and Pr exponents aren't correct for smooth turbulent flow in all fluids. In particular, the Pr exponent should be 0.6 in gasses. The present theory matches rough turbulent convection on the present apparatus within its $\pm 2.5\%$ root-sum-squared (RSS) measurement uncertainty using $\text{Pr}^{1/3}$. With $\text{Pr} = 0.71$ (air), $\text{Pr}^{0.6} \approx 0.814$ is nearly 9% smaller than $\text{Pr}^{1/3} \approx 0.892$, a deviation greater than 3 times the measurement uncertainty.

18. Conclusions

- For a plate surface with periodic, weakly isotropic roughness having RMS height-of-roughness $\varepsilon > 0$, which is inducing rough turbulence in a steady flow of strength Re, the average skin-friction coefficient and forced convection formulas are:

$$f_C = \frac{1}{3 \ln^2(L/\varepsilon)} \quad \overline{\text{Nu}} = \frac{\text{Re Pr}^{1/3}}{6 \ln^2(L/\varepsilon)} \quad \frac{L}{\varepsilon} \gg 1$$

- The periodic roughness effective period $L_P = L/\sqrt{j^2 + k^2} \ll L$, where $0 \leq j \leq w/2$ and $0 \leq k \leq w/2$ are the indexes of the $w \times w$ discrete spatial Fourier transform coefficient $X_{j,k}$ with the largest amplitude.
- A surface is weakly isotropic if its effective period $L_P \ll L$ varies less than 1.5:1 through a full rotation.
- For periodic, weakly isotropic roughness with period $L_P \ll L$, when $L_P/\varepsilon < 387$, the flow along the entire plate should transition directly from laminar to rough turbulence at $\text{Re} \approx \text{Re}_\lambda$. When $L_P/\varepsilon > 388$, then $\text{Re}_\sigma > \text{Re}_\lambda$ and the flow along the entire plate should transition from laminar to smooth turbulence at $\text{Re} \approx \text{Re}_\lambda$, and to rough turbulence at $\text{Re} \approx \text{Re}_\sigma$.

$$\text{Re}_\lambda = \left[\frac{0.664}{2\varepsilon} \right]^2 L_P L \quad \text{Re}_\sigma = \left[\frac{0.036}{2\varepsilon} \right]^5 L_P^4 L$$

- For periodic, weakly isotropic grooved plates whose flat regions are smooth, co-planar, have convex perimeters, and have area L_T^2 between cell area L_P^2 and $L_P^2/2$, the flow should be rough turbulent when $\text{Re} > \max(\text{Re}_\lambda, \text{Re}_\sigma)$ and:

$$\text{Re}_x < \text{Re}_\ell = \frac{L L_T/4}{0.036 L_P^2} \left[\frac{\varepsilon L_P}{0.036 L_T \sqrt{L_P^2 - L_T^2}} \right]^{9/4} \quad \frac{1}{2} \leq \frac{L_T^2}{L_P^2} < 1$$

- The turbulent average skin-friction coefficient and forced convection formulas for a smooth plate are:

$$f_{C\sigma} = \frac{\sqrt[3]{2}/3}{[W_0(\text{Re}/\sqrt{3}) - 1]^2} \quad \overline{\text{Nu}}_\sigma = \frac{\text{Nu}_0 \text{Re} f_{C\sigma}}{\sqrt{3}} \sqrt{\frac{\text{Pr}/9 + 1}{18 f_{C\sigma} \text{Pr} + 1}} \sqrt[3]{\frac{\text{Pr}}{\Xi \|1, 1/\text{Pr}\|_3}}$$

where W_0 is the smallest positive branch of the Lambert W function, the inverse of $\varphi \exp(\varphi)$.

$$\text{Nu}_0 = \frac{16}{\pi^2 \sqrt[4]{2}} \quad \Xi = \left\| 1, \frac{0.5}{\text{Pr}} \right\|_{\sqrt{1/3}} \quad \|\varphi, \vartheta\|_p = (|\varphi|^p + |\vartheta|^p)^{1/p} \quad \text{Re} \gg \sqrt{3}e$$

19. Nomenclature

	A	= rough plate area (m ²)
	c'_f, c_f	= local, average skin-friction coefficient Prandtl-Schlichting [1]
	$C_f/2, C_D/2$	= local, average skin-friction coefficient Mills-Hang [5]
	$C_f/2$	= local skin-friction coefficient Pimenta et al [4]
	C_m	= mean (average) skin-friction coefficient Churchill [8]
	f_c, f_C	= local, average skin-friction coefficient present work
	$G(t, w)$	= Gray-code self-similar ramp-permutation
	j_P	= index of largest $ X_j $
	k_S	= sand-roughness (m)
	L	= plate characteristic-length (m)
	L_P	= effective roughness period (m)
	L_T	= periodic flat length in direction of flow (m)
	n	= branching factor of profile roughness function
	Nu, \overline{Nu}	= local, average Nusselt number (convection)
	Pr	= Prandtl number of fluid
	$q = \log_2 w$	= positive integer
	$Ra = Gr Pr$	= Raleigh number
	Re	= Reynolds number of flow parallel to the plate
	Re_ℓ	= Re_x rough-to-smooth turbulence threshold
	Re_λ, Re_σ	= laminar, smooth turbulent Re upper-bound
	$Re_\varepsilon = v^* \varepsilon / \nu, Re_k = v^* k_S / \nu$	= roughness, sand-roughness Reynolds number
	$Re_x = x Re / L$	= local Reynolds number
	Re_0	= Re_x integration lower bound
	S_j	= compensated discrete Fourier transform coefficient
	t	= integer
	v	= bulk fluid velocity (m/s)
	v^*	= friction velocity (m/s)
	$w = 2^q$	= integer power of two
	$W(t, w)$	= wiggliest integer self-similar ramp-permutation
	W_0	= smallest positive branch of the Lambert W function
	x	= distance from leading edge of plate (m)
	$X_j, X_{j,k}$	= discrete Fourier transform coefficient
	$Y(t, w)$	= integer self-similar ramp-permutation
	z	= roughness function (m)
	\bar{z}	= mean elevation of roughness function (m)
	Z	= roughness random variable (m)

Greek Symbols

	δ_2	= momentum thickness of boundary layer flow (m)
	$\delta_{2\lambda}, \delta_{2\sigma}$	= laminar, smooth turbulent momentum thickness (m)
	ϵ, ε	= profile, surface RMS height-of-roughness (m)
	ε_{pv}	= peak to valley height-of-roughness (m)
	ν	= fluid kinematic viscosity (m ² /s)
	ρ	= fluid density (kg/m ³)
	τ	= fluid shear stress (N/m ²)

Acknowledgments

The idea of self-similar roughness grew out of a discussion with Nina Koch about turbulence self-similarity. Thanks to John Cox and Doug Ruuska for machining the bi-level plate. Thanks to Martin Jaffer for critiques and insights. Thanks to anonymous reviewers for their useful suggestions.

20. References

- [1] L. Prandtl and H. Schlichting. *The Resistance Law for Rough Plates*. Translation (David W. Taylor Model Basin). Navy Department, the David W. Taylor Model Basin, 1934. Translated 1955 by P.S. Granville.
- [2] J. Nikuradse. Laws of flow in rough pipes. *VDI Forschungsheft*, page 361, 1933. Translated 1937 by A. A. Brielmaier.
- [3] F. R. Hama. Boundary layer characteristics for smooth and rough surfaces. *Trans. Soc. Nav. Arch. Marine Engrs.*, 62:333–358, 1954.
- [4] M. M. Pimenta, R. J. Moffat, and W. M. Kays. *The Turbulent Boundary Layer: An Experimental Study of the Transport of Momentum and Heat with the Effect of Roughness*. Department of Mechanical Engineering, Stanford University, 1975.
- [5] A. F. Mills and Xu Hang. On the skin friction coefficient for a fully rough flat plate. *J. Fluids Eng*, 105(3):364–365, 1983.
- [6] Hermann Schlichting, Klaus Gersten, Egon Collaborateur. Krause, Herbert Collaborateur. Oertel, and Katherine Mayes. *Boundary-layer theory*. Springer, Berlin, Heidelberg, Paris, 2000. Corrected printing 2003.
- [7] Frank White. *Viscous Fluid Flow, 3rd Edition*. McGraw-Hill, 2006.
- [8] Stuart W. Churchill. Theoretically based expressions in closed form for the local and mean coefficients of skin friction in fully turbulent flow along smooth and rough plates. *International Journal of Heat and Fluid Flow*, 14(3):231 – 239, 1993.
- [9] Noor Afzal, Abu Seena, and A. Bushra. Turbulent flow in a machine honed rough pipe for large reynolds numbers: General roughness scaling laws. *Journal of Hydro-environment Research*, 7(1):81–90, 2013.
- [10] Karen A Flack, Michael P Schultz, Julio M Barros, and Yechan C Kim. Skin-friction behavior in the transitionally-rough regime. *International Journal of Heat and Fluid Flow*, 61:21–30, 2016.
- [11] J. H. Lienhard, IV and J. H. Lienhard, V. *A Heat Transfer Textbook*. Phlogiston Press, Cambridge, MA, 5th edition, August 2020. Version 5.10.
- [12] Mitchell G. Newberry and Van M. Savage. Self-similar processes follow a power law in discrete logarithmic space. *Phys. Rev. Lett.*, 122:158303, Apr 2019.
- [13] D. W. Smith and J. D. Walker. Skin friction measurements in incompressible flow. Technical Report R-26, NASA, Washington, DC, 1959.
- [14] D. B. Spalding and S. W. Chi. The drag of a compressible turbulent boundary layer on a smooth flat plate with and without heat transfer. *Journal of Fluid Mechanics*, 18(1):117143, 1964.
- [15] V Lienhard, John H. Heat Transfer in Flat-Plate Boundary Layers: A Correlation for Laminar, Transitional, and Turbulent Flow. *Journal of Heat Transfer*, 142(6), 04 2020. 061805.
- [16] Allan P. Colburn. A method of correlating forced convection heat-transfer data and a comparison with fluid friction. *International Journal of Heat and Mass Transfer*, 7(12):1359 – 1384, 1964.
- [17] Aubrey Jaffer. Thermodynamic basis for natural convection from an isothermal plate, 2021. <http://people.csail.mit.edu/jaffer/convect/thermo.pdf>.
- [18] Aubrey Jaffer. Convection measurement apparatus and methodology, 2021. <http://people.csail.mit.edu/jaffer/convect/measure.pdf>.